ICES REPORT 17-18

August 2017

Explicit Higher-Order Accurate Isogeometric Collocation Methods for Structural Dynamics

by

J.A. Evans, R.R. Hiemstra, T.J.R. Hughes, A. Reali

The Institute for Computational Engineering and Sciences
The University of Texas at Austin
Austin, Texas 78712

Reference: J.A. Evans, R.R. Hiemstra, T.J.R. Hughes, A. Reali, "Explicit Higher-Order Accurate Isogeometric Collocation Methods for Structural Dynamics," ICES REPORT 17-18, The Institute for Computational Engineering and Sciences, The University of Texas at Austin, August 2017.

Explicit Higher-Order Accurate Isogeometric Collocation Methods for Structural Dynamics

J.A. Evans[a,*], R.R. Hiemstra[b], T.J.R. Hughes[b], A. Reali[c,d,e]

[a]*Department of Aerospace Engineering Sciences, University of Colorado Boulder*
[b]*Institute for Computational Engineering and Sciences, The University of Texas at Austin*
[c]*Department of Civil Engineering and Architecture, University of Pavia*
[d]*Institute of Applied Mathematics and Information Technologies, National Research Council, Pavia*
[e]*Institute of Advanced Study, Technical University of Munich*

Abstract

The objective of the present work is to develop efficient, higher-order space- and time-accurate, methods for structural dynamics. To this end, we present a family of explicit isogeometric collocation methods for structural dynamics that are obtained from predictor-multicorrector schemes. These methods are very similar in structure to explicit finite-difference time-domain methods, and in particular, they exhibit similar levels of computational cost, ease of implementation, and ease of parallelization. However, unlike finite difference methods, they are easily extended to non-trivial geometries of engineering interest. To examine the spectral properties of the explicit isogeometric collocation methods, we first provide a semi-discrete interpretation of the classical predictor-multicorrector method. This allows us to characterize the spatial and modal accuracy of the isogeometric collocation predictor-multicorrector method, irrespective of the considered time-integration scheme, as well as the critical time step size for a particular explicit time-integration scheme. For pure Dirichlet problems, we demonstrate that it is possible to obtain a second-order-in-space scheme with one corrector pass, a fourth-order-in-space scheme with two corrector passes, and a fifth-order-in-space scheme with three corrector passes. For pure Neumann and mixed Dirichlet-Neumann problems, we demonstrate that it is possible to obtain a second-order-in-space scheme with one corrector pass and a third-order-in-space scheme with two corrector passes, and we observe that fourth-order-in-space accuracy may be obtained pre-asymptotically with three corrector passes. We then present second-order-in-time, fourth-order-in-time, and fifth-order-in-time fully discrete predictor-multicorrector algorithms that result from the application of explicit Runge-Kutta methods to the semi-discrete isogeometric collocation predictor-multicorrector method. We confirm the accuracy of the family of explicit isogeometric collocation methods using a suite of numerical examples.

Keywords: Isogeometric Analysis, Isogeometric Collocation, Explicit Dynamics, Predictor-Multicorrector Schemes

1. Introduction

We pursue the development of efficient, higher-order accurate, robust, explicit finite element methods for structural dynamics. There are several reasons why we see this as an opportunity at this juncture in time, and why, in our opinion, no successful methods of this type have been developed heretofore. We elaborate on these ideas in what follows.

Explicit structural dynamics methods dominate crash dynamics and metal forming simulations. They are the bread and butter of widely used commercial codes in industry, namely, LS-DYNA, and its derivatives, most notably PAM-CRASH and RADIOSS. The dominant finite element technology used in these codes is low-order four-node quadrilateral elements and low-order eight-node hexahedral elements. They

*Corresponding author. E-mail address: john.a.evans@colorado.edu

additionally employ various detailed element technologies, such as reduced and selective integration, in order to minimize storage and computational effort, and to avoid volumetric locking in continuum modeling, and shear and membrane locking in beam, plate and shell modeling (see, e.g., [21]). The well-known Central Difference Method[1], a member of the Newmark family of methods, is the time-integration method of choice in these codes (see, e.g., [12, 21]). A further element-technology simplification is also universally employed, and that is a lumped (i.e., diagonal) mass matrix, rather than a consistent mass matrix, which has the same band-profile structure as the stiffness matrix. This is done to further reduce storage and equation-solving effort. The lumped mass, in conjunction with low-order finite elements, does not reduce second-order accuracy and has the added benefit that it increases the stable critical time step, which results in increased efficiency of the algorithm. In the structural dynamics community, when we think of an explicit algorithm, we think of one that has all the aforementioned features, in particular, lumped mass.

However, strictly speaking, an algorithm for second-order-in-time, ordinary differential equations may employ a consistent mass matrix and still be considered explicit, and indeed this is the point of view of the applied mathematics numerical analysis community. For example, there are whole families of time-integration methods, such as, for example, explicit Runge-Kutta methods, that fall into this category. When applied to a second-order-in-time ordinary differential equation system, these would entail the use of whatever mass matrix was present, for example, the consistent mass as coefficient matrix of the algebraic problem that ensues within each time step. We are interested in such methods herein because we want to achieve higher-order time accuracy than second-order. A consequence is that we have to be crystal clear in the use of the terminology "explicit" and define it carefully in every use.

Another reason we are interested in using the consistent mass matrix in the present study is because, in the context of higher-order finite element methods, a universal procedure for defining diagonal mass matrices has never been developed that maintains the higher-order spatial accuracy of consistent mass and positivity of the lumped masses at the same time [Hughes, Chapter 7]. It seems to be impossible, so, if we are to achieve higher-order spatial accuracy, in addition to higher-order time accuracy, it would seem we have no other choice but to employ the consistent mass matrices. At the same time, we want to avoid the storage and equation-solving costs of consistent mass. The way we will do this will be to employ a predictor-multicorrector framework in which the corrector steps use a matrix system with a diagonal mass matrix as left-hand-side coefficient matrix, but the consistent mass matrix will be utilized to compute the right-hand-side residual forces of the dynamical system. We will show that in this way, with a sufficient, but small, number of corrector passes in each time step, we can maintain higher-order, overall spatial- and time-accuracy.

Before moving on, we need to say something about another possible terminology conflict. We have described the above approach as a "predictor-multicorrector method". However, it is not the classical structural dynamics, predictor-multicorrector method presented in [12, 21, 23, 24, 37]. In those references, one starts with an implicit method and then creates a new explicit method intimately associated with it. The approach is universal in that any implicit method can become the progenitor of a related explicit method, and this relationship can be exploited to create implicit-explicit mesh partitions in which the critical stable time step only emanates from the explicit elements. This is important, because very small and excessively stiff elements require very small time steps for stability. Those elements can be treated implicitly and their small critical time steps can be obviated thereby. The reader is referred to the references just indicated for further details. These methods have great potential in the present context, but are not the ones we are focused on herein, which are explicit Runge-Kutta methods.

What we have described so far deals with efficiencies in the treatment of the given semi-discrete (i.e., time-continuous) equations of motion. The final issue is the formation of the semi-discrete system,

[1]It is not often appreciated, but the classical Central Difference Method, strictly interpreted, is actually explicit only with respect to the stiffness term, and not the viscous damping term (see, e.g., [21]). In practice, ad hoc modifications to the algorithm are often employed to treat the viscous damping explicitly as well.

and in particular the stiffness and mass matrices, multiplied by appropriate vectors. This is not to be underestimated for several reasons. The first is that the formation of element arrays is the primary cost in explicit transient analysis, and the second is that for higher-order methods there is enormous expense associated with the formation of element arrays. We need to emphasize that by the expression "formation of element arrays" we mean the vectors of internal and inertial forces. These, and the computations of stresses by way of typically nonlinear and complex constitutive equations, constitute the entire cost of explicit structural dynamics algorithms, save for the cost of contact algorithms, which are often very important too.

Our approach to this issue is to use certain developments in Isogeometric Analysis, that is, smooth, spline-based finite elements. The first attribute of higher-order, spline-based finite elements that we wish to emphasize is their greatly superior spectral properties and likewise the inferiority of higher-order, traditional, C^0-continuous finite elements (see [13, 14, 22, 25]). The upper part of the modal spectrum for traditional C^0-continuous finite elements diverges with order elevation, in contrast with almost the entire spectrum of spline-based elements, which converges. Spline-based finite elements possess a unique combination of higher-order accuracy and robustness. These properties can be discerned from their spectral properties. As polynomial order is increased, spline-based elements become more robust, in contrast with C^0-continuous finite elements, which become less robust. This is no longer a debatable issue. The computational results unequivocally establish these facts (see [32]). Our conclusion is that there is no future for higher-order C^0-continuous finite elements in the realm of nonlinear structural dynamics analysis. This statement may be viewed as harsh, but it is supported by the fact that, after 60 years of intense development of the finite element method, there appears to be no past evidence to contradict it.

The final issue that we need to deal with is the cost of formation of element arrays. Naïve implementations of spline-based finite elements can be excessively costly, and can increase dramatically as polynomial order is increased. Recently, it has been shown that one can take advantage of smoothness to develop very fast procedures to generate arrays. There have been two major developments: One is within the classical Galerkin framework (see [2, 3, 7, 10, 20, 26, 27, 36]), and the other involves collocation, that is utilizing the strong form of the equations (see [4, 5, 11, 35, 39]). Both have merit for the objectives described previously but, in this paper, we will focus on the latter. The idea of a variational collocation method is to take advantage of smoothness of the spline basis functions and integrate-by-parts, under the integral sign, to obtain the strong variational form in which weighting functions are undifferentiated. Then, essentially a one-point element integration rule is used to evaluate arrays, independent of the polynomial order of the elements. This is remarkable in that the resulting discrete equations for smooth splines can be shown to be stable, assuming the collocation points are appropriately selected. This issue will not discussed further here, but rather we refer to original works (see [18, 26, 38]]). The upshot is, spline-based collocation is a very efficient technology for element formation in higher-order dynamic analysis. It has also been shown that collocated spline approaches have superior spectral approximation properties over C^0-continuous finite elements, similar to those of Galerkin spline-based elements (see [5]). This and all the above described methodologies are combined in this work to achieve efficient, higher-order accurate, explicit finite element methods for structural dynamics.

The new methods require only $O\left((p+1)^d\right)$ floating point operations per-degree-of-freedom for system formation, and they are truly explicit in that they do not require the solution of a linear system at each time step. Our methods exhibit up to fifth-order accuracy in space for pure Dirichlet problems provided that a suitable but low number of corrector passes are employed, and they admit relaxed time step restrictions even when compared with an isogeometric Galerkin formulation. The methods are additionally characterized by a simple equation-by-equation assembly structure, resulting in efficient implementation and high levels of parallel scalability. In fact, they exhibit similar levels of computational cost, ease of implementation, and ease of parallelization to those of finite-difference time-domain methods. However, in contrast with finite-difference time-domain methods, our methods easily extend to complicated geometries of real-world engineering complexity without any additional machinery.

One of the important contributions of this work is the identification of predictor-multicorrector methods as certain semi-discrete methods. This facilitates the theoretical analysis of predictor-multicorrector methods that has been heretofore difficult, if not impossible. Previously, only the simplest cases, involving one, or at most two, corrector passes yielded to analysis. We are thus able to give precise descriptions of the frequency spectra, and the phase and amplitude errors, produced by these methods.

An outline of the remainder of the paper is as follows. In Section 2, we give a brief overview of isogeometric collocation as applied to the linear elastodynamics problem. In Section 3, we present a semi-discrete interpretation of the classical predictor-multicorrector method, and in Section 4, we characterize the spatial and modal accuracy of the semi-discrete isogeometric collocation predictor-multicorrector method. In Section 5, we present our family of explicit isogeometric collocation methods that are obtained by applying common explicit time-integration schemes to the semi-discrete isogeometric collocation predictor-multicorrector method. In particular, we present second-order-in-time, fourth-order-in-time, and fifth-order-in-time fully discrete predictor-multicorrector algorithms that result from the application of explicit Runge-Kutta time integration. In Section 6, we discuss the critical time-step size associated with our fully discrete predictor-multicorrector algorithms, and we also provide a detailed assessment of computational cost. In Section 7, we present a suite of numerical experiments that illustrate the performance of our explicit isogeometric collocation methods. Finally, in Section 8, we draw conclusions.

2. Isogeometric Collocation Methods for Linear Elastodynamics

In this section, we give a brief review of isogeometric collocation as applied to the linear elastodynamics problem. We first state the strong form of the linear elastodynamics problem before presenting its spatial discretization by an isogeometric collocation scheme.

2.1. The Strong Form of the Linear Elastodynamics Problem

The strong form of the linear elastodynamics initial-boundary value problem is as follows:

$$(S)\begin{cases} \text{Find } \mathbf{u} : \overline{\Omega} \times [0,T] \to \mathbb{R}^d \text{ such that} & & \\ \rho\ddot{\mathbf{u}}(\mathbf{x},t) = \nabla \cdot \boldsymbol{\sigma}(\mathbf{x},t) + \mathbf{f}(\mathbf{x},t) & \forall \mathbf{x} \in \Omega, t \in (0,T) & (2.1)\\ \mathbf{u}(\mathbf{x},t) = \mathbf{g}(\mathbf{x},t) & \forall \mathbf{x} \in \Gamma_g, t \in (0,T) & (2.2)\\ \boldsymbol{\sigma}(\mathbf{x},t)\cdot\mathbf{n} = \mathbf{h}(\mathbf{x},t) & \forall \mathbf{x} \in \Gamma_h, t \in (0,T) & (2.3)\\ \mathbf{u}(\mathbf{x},0) = \mathbf{u}_0(\mathbf{x}) & \forall \mathbf{x} \in \Omega & (2.4)\\ \dot{\mathbf{u}}(\mathbf{x},0) = \mathbf{v}_0(\mathbf{x}) & \forall \mathbf{x} \in \Omega & (2.5) \end{cases}$$

Above, $\Omega \subset \mathbb{R}^d$ is the spatial domain of the problem, d is the number of spatial dimensions, Γ is the boundary of the domain, Γ_g is the Dirichlet part of the boundary, Γ_h is the Neumann part of the boundary, $\mathbf{n}$ is unit outward boundary normal, $\mathbf{u}$ is the displacement field, $\boldsymbol{\sigma}$ is the Cauchy stress tensor, ρ is the density, $\mathbf{g}$ is the prescribed displacement along Γ_g, $\mathbf{h}$ is the prescribed traction along Γ_h, $\mathbf{f}$ is the applied forcing, $\mathbf{u}_0$ is the initial displacement field, and $\mathbf{v}_0$ is the initial velocity field. In the linear setting, the Cauchy stress tensor is given by the generalized Hooke's law:

$$\boldsymbol{\sigma} = \mathbb{C}\nabla^s\mathbf{u}$$

where $\mathbb{C}$ is the fourth-order stiffness tensor and $\nabla^s\mathbf{u} = \frac{1}{2}\left(\nabla\mathbf{u} + (\nabla\mathbf{u})^T\right)$ is the infinitesimal strain tensor. The elastic coefficients of the stiffness tensor are assumed to satisfy standard symmetry and positive-definiteness conditions [21, Chapter 2].

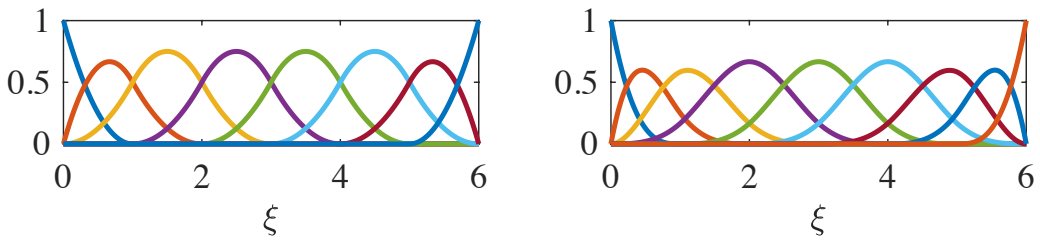

Figure 1: Maximal continuity univariate B-spline basis functions of degree $p = 2$ (left) and $p = 3$ (right).

2.2. The Isogeometric Collocated Semi-Discrete Form of the Linear Elastodynamics Problem

Now that we have stated the strong form of the linear elastodynamics problem, we are ready to discuss its approximation by means of the isogeometric collocation method [4]. There are two basic ingredients in the isogeometric collocation method: (i) a set of basis functions for spatial approximation of the displacement field and (ii) a set of collocation points at which the strong form of the linear elastodynamics problem will be satisfied.

With regard to spatial approximation, we use non-uniform rational B-spline (NURBS) basis functions, though T-spline [11], hierarchical B-spline [39], or generalized B-spline [35] basis functions may also be employed. NURBS basis functions are defined in terms of B-spline basis functions, and B-spline basis functions in turn are first built on a parametric domain $\hat{\Omega} = (0,1)^d$ given a collection of polynomial degrees p_A and knot vectors Ξ_A in each parametric direction $A = 1, \ldots, d$. The construction of B-spline basis functions is well-known, so we refer the reader to [12, Chapter 2] for more details. Maximal continuity univariate B-spline basis functions are illustrated in Fig. 1. We denote B-spline basis functions in the parametric domain as $\left\{\hat{N}_i(\boldsymbol{\xi})\right\}_{i=1}^{N_{\text{basis}}}$ where N_{basis} is the total number of basis functions. NURBS basis functions are then defined using a projective transformation:

$$\hat{R}_i(\boldsymbol{\xi}) = \frac{w_i \hat{N}_i(\boldsymbol{\xi})}{\sum_{j=1}^{N_{\text{basis}}} w_j \hat{N}_j(\boldsymbol{\xi})} \qquad \forall \boldsymbol{\xi} \in \hat{\Omega}$$

where $\{w_i\}_{i=1}^{N_{\text{basis}}}$ is a set of positive weights. In the isogeometric setting, the spatial domain is assumed to be defined by a NURBS parametric mapping $\mathbf{F} : \hat{\Omega} \to \Omega$ of the form:

$$\mathbf{F}(\boldsymbol{\xi}) = \sum_{i=1}^{N_{\text{basis}}} \mathbf{P}_i \hat{R}_i(\boldsymbol{\xi}) \qquad \forall \boldsymbol{\xi} \in \hat{\Omega} \tag{2.6}$$

where $\{\mathbf{P}_i\}_{i=1}^{N_{\text{basis}}}$ is a set of control points. Finally, NURBS basis functions in the physical domain are defined using the pull back operator, namely:

$$R_i(\mathbf{x}) = \hat{R}_i\left(\mathbf{F}^{-1}(\mathbf{x})\right) \qquad \forall \mathbf{x} \in \Omega$$

for $i = 1, \ldots, N_{\text{basis}}$, and we denote the space of NURBS approximation functions as:

$$\mathcal{V}^h = \text{span}\left(\{R_i(\mathbf{x})\}_{i=1}^{N_{\text{basis}}}\right)$$

We further denote the space of displacement approximation functions as:

$$\boldsymbol{\mathcal{V}}_T^h = \left\{\mathbf{u}^h : \overline{\Omega} \times [0,T] \to \mathbb{R}^d : u_A^h(\cdot, t) \in \mathcal{V}^h \text{ for } A = 1, 2, \ldots, d \text{ and } t \in (0,T)\right\}$$

With regard to collocation points, we may turn to several different candidates, including Cauchy-Galerkin points [18], Demko abscissae [16], and Greville abscissae [28]. A collocation scheme based on

Cauchy-Galerkin points exhibits optimal convergence rates, but Cauchy-Galerkin points are problem-dependent and must be approximated in practice [38]. Consequently, we do not consider them further in this paper. Demko abscissae are stable for any mesh and polynomial degree in one spatial dimension, but they are quite costly to compute. Greville abscissae, on the other hand, are easily computable from the knot vectors underlying a NURBS discretization, though they are unstable for certain geometrically graded meshes and very high polynomial degree. In practice, isogeometric collocation methods based on Demko and Greville abscissae yield results of comparable accuracy [4], so we will employ Greville abscissae in all of our subsequent numerical experiments. We denote the Greville abscissae in parametric space as $\hat{\boldsymbol{\tau}}_i$ for $i = 1, \ldots, N_{\text{basis}}$, and Greville abscissae in physical space are defined using the push forward:

$$\boldsymbol{\tau}_i = \mathbf{F}(\hat{\boldsymbol{\tau}}_i)$$

We will need to distinguish between collocation points on the interior, the Dirichlet boundary, and the Neumann boundary. Thus, we define the sets of indices:

$$\begin{aligned} \eta_{int} &:= \{i \in \{1, \ldots, N_{\text{basis}}\} : \boldsymbol{\tau}_i \in \Omega\}, \\ \eta_g &:= \{i \in \{1, \ldots, N_{\text{basis}}\} : \boldsymbol{\tau}_i \in \Gamma_g\} \\ \eta_h &:= \{i \in \{1, \ldots, N_{\text{basis}}\} : \boldsymbol{\tau}_i \in \Gamma_h\} \end{aligned}$$

corresponding to interior, Dirichlet, and Neumann collocation points respectively.

We are now ready to state the isogeometric collocated semi-discrete form of the linear elastodynamics problem. We collocate the partial differential equation (2.1) at interior collocation points, the acceleration Dirichlet boundary condition implied by (2.2) at Dirichlet collocation points, and a linear combination of the partial differential equation (2.1) and Neumann boundary condition (2.3) at Neumann collocation points using the so-called enhanced collocation technique [15]. The enhanced collocation technique is critical to our development of a fully explicit scheme, as will be elaborated later. Moreover, we collocate the initial conditions (2.4) and (2.5) at all collocation points. The corresponding semi-discrete problem takes the form:

$$(C) \begin{cases} \text{Find } \mathbf{u}^h \in \boldsymbol{\mathcal{V}}_T^h \text{ such that:} & \\ \rho \ddot{\mathbf{u}}^h(\boldsymbol{\tau}_i, t) = \nabla \cdot \Big(\mathbb{C} \nabla^s \mathbf{u}^h(\boldsymbol{\tau}_i, t) \Big) + \mathbf{f}(\boldsymbol{\tau}_i, t) & \forall i \in \eta_{int}, t \in (0, T) \quad (2.7) \\ \rho \ddot{\mathbf{u}}^h(\boldsymbol{\tau}_i, t) = \rho \ddot{\mathbf{g}}(\boldsymbol{\tau}_i, t) & \forall i \in \eta_g, t \in (0, T) \quad (2.8) \\ \rho \ddot{\mathbf{u}}^h(\boldsymbol{\tau}_i, t) = \nabla \cdot \Big(\mathbb{C} \nabla^s \mathbf{u}^h(\boldsymbol{\tau}_i, t) \Big) + \mathbf{f}(\boldsymbol{\tau}_i, t) & \\ \qquad - \dfrac{C^*}{h^*} \Big(\mathbb{C} \nabla^s \mathbf{u}^h(\boldsymbol{\tau}_i, t) \cdot \mathbf{n} - \mathbf{h}(\boldsymbol{\tau}_i, t) \Big) & \forall i \in \eta_h, t \in (0, T) \quad (2.9) \\ \mathbf{u}^h(\boldsymbol{\tau}_i, 0) = \mathbf{u}_0(\boldsymbol{\tau}_i) & \forall i \in \{1, \ldots, N_{\text{basis}}\} \quad (2.10) \\ \dot{\mathbf{u}}^h(\boldsymbol{\tau}_i, 0) = \mathbf{v}_0(\boldsymbol{\tau}_i) & \forall i \in \{1, \ldots, N_{\text{basis}}\} \quad (2.11) \end{cases}$$

Above, C^* is a suitably chosen positive constant and h^* is the mesh size perpendicular to the boundary at a given Neumann collocation point [15]. The above problem consists of a linear system of ordinary differential equations. It should be noted that our approach to boundary condition enforcement results in a mass associated with each and every collocation point. This will prove critical in the development of explicit isogeometric collocation methods, since even the boundary conditions are expressed in terms of ordinary differential equations.

We can also write the isogeometric collocated semi-discrete form of the linear elastodynamics problem in terms of a matrix system which will prove useful in our later discussion. In this direction, let us first define a destination array which takes in a coordinate direction $A = 1, \ldots, d$ and a basis function or control point index $i = 1, \ldots, N_{\text{basis}}$ and returns a degree of freedom index P [21, Chapter 2]:

$$P = \text{ID}(A, i)$$

With such a connectivity array in place, define M to be a mass matrix satisfying:

$$[\mathsf{M}]_{PQ} = R_j(\boldsymbol{\tau}_i)\delta_{AB}$$

where $P = \mathrm{ID}(A,i)$, $Q = \mathrm{ID}(B,j)$, and δ_{AB} is the Kronecker delta. Define K to be a stiffness matrix satisfying:

$$[\mathsf{K}]_{PQ} = \begin{cases} \mathbf{e}_A \cdot (-\nabla \cdot (\mathbb{C}\nabla^s (R_j(\boldsymbol{\tau}_i)\mathbf{e}_B))) & \text{if } i \in \eta_{int} \\ 0 & \text{if } i \in \eta_g \\ \mathbf{e}_A \cdot \left(-\nabla \cdot (\mathbb{C}\nabla^s (R_j(\boldsymbol{\tau}_i)\mathbf{e}_B)) + \frac{C^*}{h^*}\left(\mathbb{C}\nabla^s \left(R_j^h(\boldsymbol{\tau}_i)\mathbf{e}_B\right)\cdot \mathbf{n}\right)\right) & \text{if } i \in \eta_h \end{cases}$$

where $\mathbf{e}_A$ and $\mathbf{e}_B$ are Cartesian unit vectors, and define F to be a forcing vector satisfying:

$$[\mathsf{F}]_P(t) = \begin{cases} f_A(\boldsymbol{\tau}_i, t) & \text{if } i \in \eta_{int} \\ \rho \ddot{g}_A(\boldsymbol{\tau}_i, t) & \text{if } i \in \eta_g \\ \frac{C^*}{h} h_A(\boldsymbol{\tau}_i, t) & \text{if } i \in \eta_h \end{cases}$$

Moreover, let us write the isogeometric displacement field as:

$$\mathbf{u}^h(\mathbf{x}, t) = \sum_{i=1}^{N_{\text{basis}}} \mathbf{u}_i(t) R_i(\mathbf{x})$$

such that we can define a solution vector $\overline{\mathbf{u}}$ satisfying:

$$[\overline{\mathbf{u}}]_Q(t) = \mathbf{e}_B \cdot \mathbf{u}_j(t)$$

Finally, define appropriate initial displacement and velocity vectors $\overline{\mathbf{u}}_0$ and $\overline{\mathbf{v}}_0$ such that (2.10) and (2.11) are satisfied. With all the aforementioned machinery in place, the matrix form of the isogeometric semi-discrete problem is:

$$(M) \begin{cases} \text{Find } \overline{\mathbf{u}} : (0,T) \to \mathbb{R}^N \text{ such that:} & \\ \mathsf{K}\overline{\mathbf{u}}(t) + \mathsf{M}\dfrac{d^2}{dt^2}\overline{\mathbf{u}}(t) = \mathsf{F}(t) \qquad \forall t \in (0,T) & (2.12) \\ \overline{\mathbf{u}}(t=0) = \overline{\mathbf{u}}_0 & (2.13) \\ \dfrac{d}{dt}\overline{\mathbf{u}}(t=0) = \overline{\mathbf{v}}_0 & (2.14) \end{cases}$$

Above, $N = N_{\text{basis}} \times d$ is the total number of degrees of freedom in the semi-discrete system. Before proceeding forward, it is useful to note two items. First, the system mass matrix consists solely of non-negative entries, and the diagonal lumped mass matrix formed by summing the rows of the mass matrix is precisely the identity matrix. These properties follow from the fact that NURBS basis functions are non-negative and form a partition of unity. If we elected to employ a basic collocation treatment of the Neumann boundary condition (corresponding to $C^* = 0$), then the corresponding mass matrix would not be invertible and explicit time-integration would not be properly defined. Second, neither the system mass matrix nor the system stiffness matrix are guaranteed to be symmetric or even have real, non-negative eigenvalues. However, for practical polynomial degrees and meshes, the two matrices are at least observed to have real, non-negative eigenvalues.

N	$p=2$	$p=3$	$p=4$	$p=5$	$p=6$
10	0.5000	0.6814	0.8120	0.8904	0.9403
20	0.5000	0.6780	0.8067	0.8828	0.9299
30	0.5000	0.6777	0.8063	0.8824	0.9293
40	0.5000	0.6776	0.8062	0.8823	0.9293
50	0.5000	0.6776	0.8062	0.8823	0.9293
60	0.5000	0.6776	0.8062	0.8823	0.9293
70	0.5000	0.6776	0.8062	0.8823	0.9293
80	0.5000	0.6776	0.8062	0.8823	0.9293
90	0.5000	0.6776	0.8062	0.8823	0.9293
100	0.5000	0.6776	0.8062	0.8823	0.9293

Table 1: Values of $\rho(\mathsf{A})$ corresponding to a 1D isogeometric collocation scheme.

3. Semi-Discrete Reinterpretation of the Predictor-Multicorrector Approach

If an explicit time-integration scheme is applied to the semi-discrete system given by (2.12)-(2.14), then one must solve a mass matrix system of the following form at each time-step:

$$\mathsf{M}\mathbf{x} = \mathbf{b} \tag{3.1}$$

In the predictor-multicorrector approach, the mass matrix is replaced by a matrix of simpler structure, namely the lumped mass matrix, in order to reduce the computational cost associated with this inversion. This results in the following iterative scheme:

$$\begin{cases} \mathbf{x}^{(0)} = \mathbf{0}, \\ \text{for } i = 0, \ldots, r-1 \\ \qquad \mathsf{M}_L \Delta\mathbf{x}^{(i)} = \mathbf{b} - \mathsf{M}\mathbf{x}^{(i)} \\ \qquad\quad \mathbf{x}^{(i+1)} = \mathbf{x}^{(i)} + \Delta\mathbf{x}^{(i)} \\ \text{end} \end{cases} \tag{3.2}$$

where M_L denotes the lumped mass matrix and r denotes the number of corrector passes. This iterative scheme relies on the recurrence relation:

$$\mathsf{M}_L \mathbf{x}^{(i+1)} = \mathbf{b} - \mathsf{A}\mathsf{M}_L \mathbf{x}^{(i)} \tag{3.3}$$

wherein $\mathsf{A} = \mathsf{M}\mathsf{M}_L^{-1} - \mathsf{I}$. Thus, the predictor-multicorrector approach to solving (3.1) may be viewed as a stationary iterative method akin to the Jacobi or Gauss-Seidel method, and we can guarantee that the predictor-multicorrector method converges if the spectral radius of the iteration matrix is less than 1.0. That is, we can guarantee convergence if:

$$\rho(\mathsf{M}_L^{-1}\mathsf{A}\mathsf{M}_L) < 1 \tag{3.4}$$

If the lumped mass matrix is the identity matrix, as is the case with isogeometric collocation, then convergence is guaranteed if $\rho(\mathsf{A}) = \rho(\mathsf{M} - \mathsf{I}) < 1$. In Table 1, computed values of $\rho(\mathsf{A})$ are reported for a selection of 1D isogeometric collocation schemes. From the table, it is apparent that the spectral radius is less than 1.0 for all considered cases, and the predictor-multicorrector method is guaranteed to converge.

In practice, we are not interested in converging the predictor-multicorrector method to some prescribed tolerance but instead utilizing a fixed number of corrector passes. To study the spectral properties of

such a method, it is useful to recast the predictor-multicorrector method into an alternate form. Utilizing (3.3) recursively yields:

$$\begin{aligned}
\mathsf{M}_L\mathbf{x}^{(r)} &= \mathbf{b} - \mathsf{A}\mathsf{M}_L\mathbf{x}^{(r-1)} \\
&= \mathbf{b} - \mathsf{A}\left(\mathbf{b} - \mathsf{A}\mathsf{M}_L\mathbf{x}^{(r-2)}\right) \\
&= \mathbf{b} - \mathsf{A}\mathbf{b} + \mathsf{A}^2\left(\mathbf{b} - \mathsf{A}\mathsf{M}_L\mathbf{x}^{(r-3)}\right) \\
&\quad\vdots \\
&= \mathbf{b} - \mathsf{A}\mathbf{b} + \mathsf{A}^2\mathbf{b} - \mathsf{A}^3\mathbf{b} + \ldots + (-1)^{r-1}\mathbf{A}^{r-1}\left(\mathbf{b} - \mathsf{M}_L\mathbf{x}^{(0)}\right) \\
&= \mathbf{b} - \mathsf{A}\mathbf{b} + \mathsf{A}^2\mathbf{b} - \mathsf{A}^3\mathbf{b} + \ldots + (-1)^{r-1}\mathbf{A}^{r-1}\mathbf{b} \\
&= \left(\sum_{i=0}^{r-1}(-1)^i\mathsf{A}^i\right)\mathbf{b}
\end{aligned} \tag{3.5}$$

In the above, we have used $\mathbf{x}^{(0)} = \mathbf{0}$. Consequently, the r-pass predictor-multicorrector method may be viewed as replacing the linear system given in (3.1) with:

$$\mathsf{M}_r\mathbf{x} = \mathbf{b} \tag{3.6}$$

where:

$$\mathsf{M}_r := \left(\sum_{i=0}^{r-1}(-1)^i\mathsf{A}^i\right)^{-1}\mathsf{M}_L \tag{3.7}$$

This view allows us to reinterpret the role of predictor-multicorrector methods in time-integration. Rather than applying the predictor-multicorrector method to a particular time-integration scheme, we can instead directly apply the predictor-multicorrector method to the semi-discrete equations of motion. In the context of elastodynamics, the resulting semi-discrete predictor-multicorrector system takes the form:

$$\mathsf{K}\overline{\mathbf{u}} + \mathsf{M}_r\frac{d^2}{dt^2}\overline{\mathbf{u}} = \mathsf{F} \tag{3.8}$$

We can then apply whatever time-integration scheme we desire to the above system. This viewpoint not only allows us to generalize the predictor-multicorrector method to arbitrary time-integration schemes, but it also enables study of the underlying spectral properties of the predictor-multicorrector approach. We can compare the discrete eigenvalues and eigenvectors associated with (3.8) and the corresponding eigenvalues and eigenvectors associated with the continuous system. This will enable us to characterize the spatial and modal accuracy of the predictor-multicorrector method, irrespective of the considered time-integration scheme, as well as the critical time step size for a particular predictor-multicorrector explicit time-integration scheme.

4. Spectral Properties of the Semi-Discrete Predictor-Multicorrector Method

To assess the accuracy of the semi-discrete predictor-multicorrector method, we examine the accuracy of the eigenfrequencies and eigenfunctions associated with the eigenproblem: For $n = 1, 2, \ldots, N$, find eigenvalues $\lambda_n^h \in \mathbb{R}^+$ and eigenvectors $\overline{\mathbf{u}}_n \in \mathbb{R}^N$ such that:

$$\mathsf{K}\overline{\mathbf{u}}_n = \lambda_n^h\mathsf{M}_r\overline{\mathbf{u}}_n \tag{4.1}$$

For a stable collocation method[2], the eigenvalues are real, ordered, and satisfy $0 \leq \lambda_1^h \leq \lambda_2^h \leq \ldots \leq \lambda_N^h$[3]. The eigenfrequencies associated with the eigenproblem are $\omega_n^h = \left(\lambda_n^h\right)^{-1/2}$ for $n = 1, \ldots, N$, and the n^{th} eigenvector $\overline{\mathbf{u}}_n$ corresponds to the vector of control variables for the discrete eigenfunction $\mathbf{u}_n^h : \Omega \to \mathbb{R}^d$. It is well-known that the solution to (3.8) may be written in terms of the eigenfrequencies and eigenfunctions of (4.1), and in fact, the error of the solution to (3.8) may be bounded by the eigenfrequency and eigenfunction errors [22]. Indeed, if there exists an integer q such that for each $n = 1, 2, \ldots, \infty$, there exists an $h_n > 0$ such that:

$$\left|\omega_n^h - \omega_n\right| \lesssim h^q \omega_n \tag{4.2}$$

$$\left\|u_n^h - u_n\right\|_{L^2(\Omega)} \lesssim h^q \left\|u_n\right\|_{L^2(\Omega)} \tag{4.3}$$

for $h < h_n$ where h is the global mesh size (defined as the greatest distance between adjacent collocation points), then for each $t \in (0, T)$, the following bound holds:

$$\left\|u^h(t) - u(t)\right\|_{L^2(\Omega)} \lesssim h^q |||u||| \tag{4.4}$$

where $|||\cdot|||$ is a suitable space-time norm [22]. Above, ω_n and u_n denote the exact n^{th} largest eigenfrequency and eigenfunction, respectively, and u denotes the exact solution to the original problem.

In structural dynamics, we are not only interested in the approximation of individual eigenfrequencies and eigenfunctions, but rather the entire spectrum. This is especially important in nonlinear problems wherein the low-, medium-, and high-frequency modes interact. To examine the spectrum in its entirety for a simple model problem, we have computed the discrete eigenfrequencies and eigenfunctions resulting from applying a 1D isogeometric collocation scheme to the pure Dirichlet 1D eigenproblem: Find eigenvalues λ_n and eigenvectors u_n such that:

$$-\frac{d^2 u_n}{dx^2} = \lambda_n u_n \tag{4.5}$$

in $\Omega = (0, 1)$ subject to the boundary conditions $u_n(0) = u_n(1) = 0$. The exact solution to this problem is $(u_n(x), \lambda_n) = \left(\sin(n\pi x), (n\pi)^2\right)$ for $n = 1, 2, \ldots, \infty$. In Fig. 2(a), we have compared the discrete eigenfrequencies with the exact eigenfrequencies for $N = 1000$ when the consistent mass matrix has been employed. Note that as the polynomial degree is increased, the spectrum uniformly converges with the exception of a finite number of outlier modes. In Fig. 2(b), we have compared the discrete eigenfrequencies with the exact eigenfrequencies for $N = 1000$ when the consistent mass matrix has been replaced by a single pass of the predictor-multicorrector algorithm. In this setting, the discrete eigenfrequencies do *not* improve with increased polynomial degree. Indeed, the spectrum appears to worsen with increased polynomial degree. In Fig. 2(c), we have compared the discrete eigenfrequencies with the exact eigenfrequencies for $N = 1000$ when the consistent mass matrix has been replaced by two passes of the predictor-multicorrector algorithm. The discrete eigenfrequencies reported here are more accurate than the eigenfrequencies associated with the single pass algorithm, especially for the low frequencies. Indeed, it can be seen that the low eigenfrequencies associated with polynomial degree $p > 2$ are more accurate than the low eigenfrequencies associated with degree $p = 2$. However, the low frequencies associated with polynomial degree $p > 4$ are not necessarily more accurate than the low eigenfrequencies associated with degree $p = 4$. In Fig. 2(d), we have compared the discrete eigenfrequencies with the exact

[2]We say a collocation method for the structural dynamics method is stable if the numerical solution remains uniformly bounded for all time in the absence of an applied forcing.

[3]Due to our method of boundary condition enforcement, there will be zero eigenvalues associated with each Dirichlet collocation point. When comparing discrete spectra with their continuous counterpart, we ignore these eigenvalues.

eigenfrequencies for $N = 1000$ when the consistent mass matrix has been replaced by three passes of the predictor-multicorrector algorithm. Again, the discrete eigenfrequencies reported here are more accurate than the eigenfrequencies associated with either the single pass or double pass algorithms, especially for the low frequencies. The low eigenfrequencies associated with polynomial degree $p > 2$ are more accurate than the low eigenfrequencies associated with degree $p = 2$, and the low eigenfrequencies associated with polynomial degree $p > 4$ are more accurate than the low eigenfrequencies associated with degree $p = 4$. We also compared the discrete eigenfrequencies with the exact eigenfrequencies for $N = 1000$ when the consistent mass matrix has been replaced by four or five passes of the predictor-multicorrector algorithm, and these results are displayed in Fig. 2(e) and 2(f), respectively. We observe from these figures that the spectrum uniformly improves with an increasing number of passes.

Now that we have examined the entire spectrum for the pure 1D Dirichlet eigenproblem, let us turn back to our discussion of accuracy. Recall that if the rate of convergence of each eigenfrequency and eigenfunction is order q, then the semi-discrete solution to the structural dynamics problem also exhibits a rate of convergence of order q. With this in mind, we have computed the errors of the first three eigenfrequencies resulting from the application of a 1D isogeometric collocation scheme to (4.5). In our calculations, we have replaced the consistent mass matrix by a select number of passes of the predictor-multicorrector algorithm. In Fig. 3, we have reported errors in the first frequency versus mesh size for a 1D collocation collocation scheme for polynomial degrees $p = 2$, 4, and 6. From this figure, we observe that the eigenfrequency is second-order accurate for $p = 2$ no matter how many passes are conducted. For $p = 4$, the eigenfrequency is second-order accurate if only one pass is conducted, while it is fourth-order accurate if more than one pass is conducted. Finally, for $p = 6$, the eigenfrequency is second-order accurate if one pass is conducted, fourth-order accurate if two passes are conducted, and fifth-order accurate if more than two passes are conducted. From our numerical computations, it appears that sixth-order accuracy is not possible using a fixed number of passes. In Fig. 4 and 5, we have reported errors in the second and third frequencies, respectively, versus mesh size for a 1D collocation collocation scheme for polynomial degrees $p = 2$, 4, and 6. These results are similar to those displayed in Fig. 3. We have conducted a number of additional numerical experiments and have observed the following behavior in the frequency error:

$$\frac{\left|\omega_n^h - \omega_n\right|}{\omega_n} \approx \begin{cases} h^2 & \text{if } p = 2, 3 \text{ or } p > 3 \text{ with only one pass} \\ h^4 & \text{if } p = 4, 5 \text{ with at least two passes or } p > 5 \text{ with only two passes} \\ h^5 & \text{if } p > 5 \text{ with at least three passes} \end{cases} \tag{4.6}$$

Moreover, we have observed similar behavior in the eigenfunction error, namely:

$$\frac{\left\|u_n^h - u_n\right\|_{L^2(\Omega)}}{\left\|u_n\right\|_{L^2(\Omega)}} \approx \begin{cases} h^2 & \text{if } p = 2, 3 \text{ or } p > 3 \text{ with only one pass} \\ h^4 & \text{if } p = 4, 5 \text{ with at least two passes or } p > 5 \text{ with only two passes} \\ h^5 & \text{if } p > 5 \text{ with at least three passes} \end{cases} \tag{4.7}$$

Consequently, we anticipate the following error estimate to hold for the semi-discrete predictor-multicorrector method as applied to the pure Dirichlet problem: For each $t \in (0, T)$, we have:

$$\frac{\left\|u^h(t) - u_n(t)\right\|_{L^2(\Omega)}}{|||u|||} \approx \begin{cases} h^2 & \text{if } p = 2, 3 \text{ or } p > 3 \text{ with only one pass} \\ h^4 & \text{if } p = 4, 5 \text{ with at least two passes or } p > 5 \text{ with only two passes} \\ h^5 & \text{if } p > 5 \text{ with at least three passes} \end{cases} \tag{4.8}$$

In the fully discrete setting, it will be advantageous to utilize a time-integration scheme with the same order of convergence as the semi-discrete method. We therefore present a number of different time-integration methods in the next section to properly balance the temporal discretization error and the spatial discretization error.

To examine the impact of alternative sets of boundary conditions, we have also computed the discrete eigenvalues and eigenfunctions resulting from applying a 1D isogeometric collocation scheme to the pure

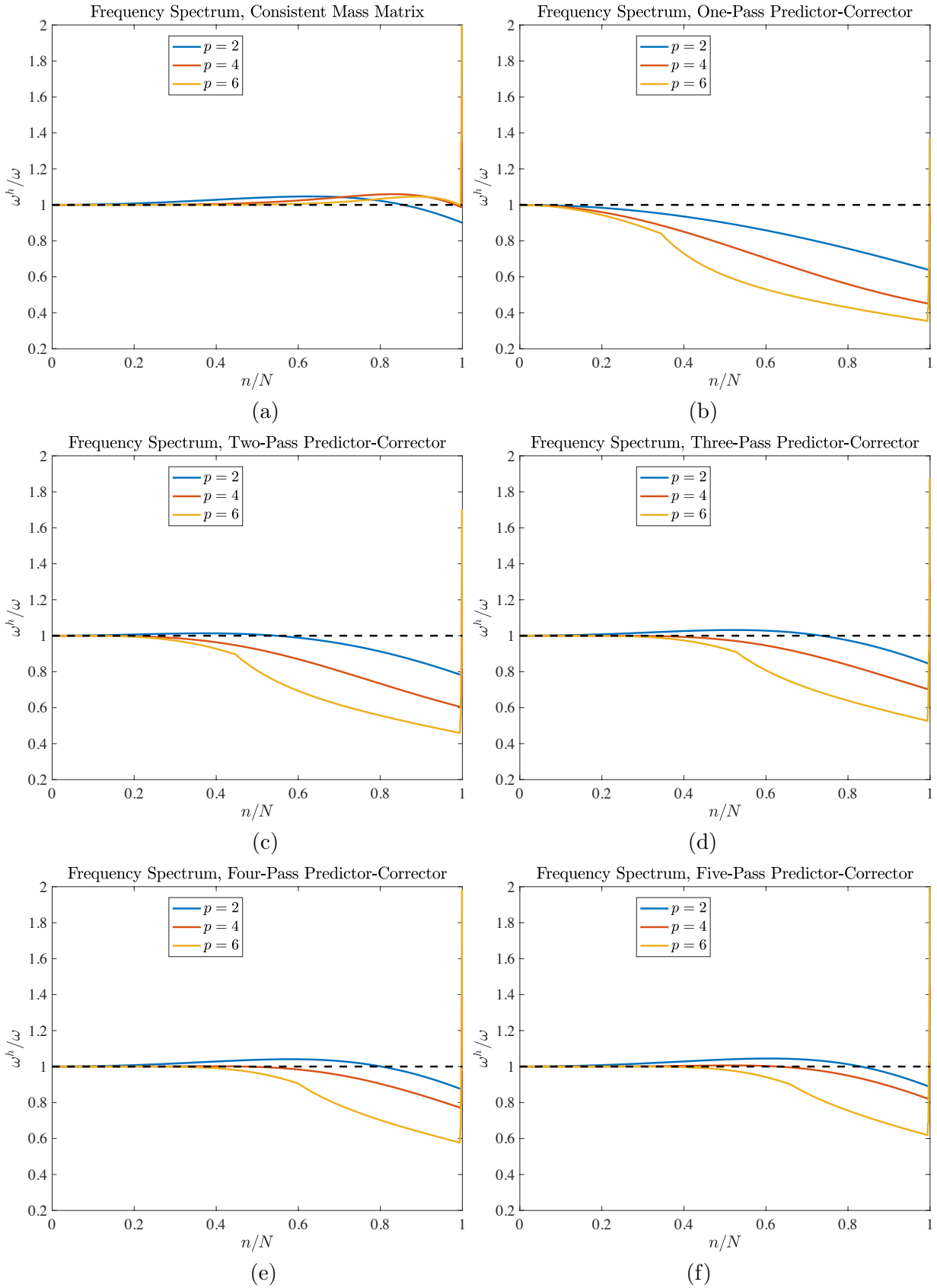

Figure 2: Eigenfrequency spectrum for a 1D isogeometric collocation scheme as applied to a pure Dirichlet problem when (a) the consistent mass matrix is employed, (b) one pass is employed in a predictor-multicorrector algorithm, (c) two passes are employed in a predictor-multicorrector algorithm, (d) three passes are employed in a predictor-multicorrector algorithm, (e) four passes are employed in a predictor-multicorrector algorithm, and (f) five passes are employed in a predictor-multicorrector algorithm. The dashed black lines in the above plots correspond to $\omega^h/\omega = 1$.

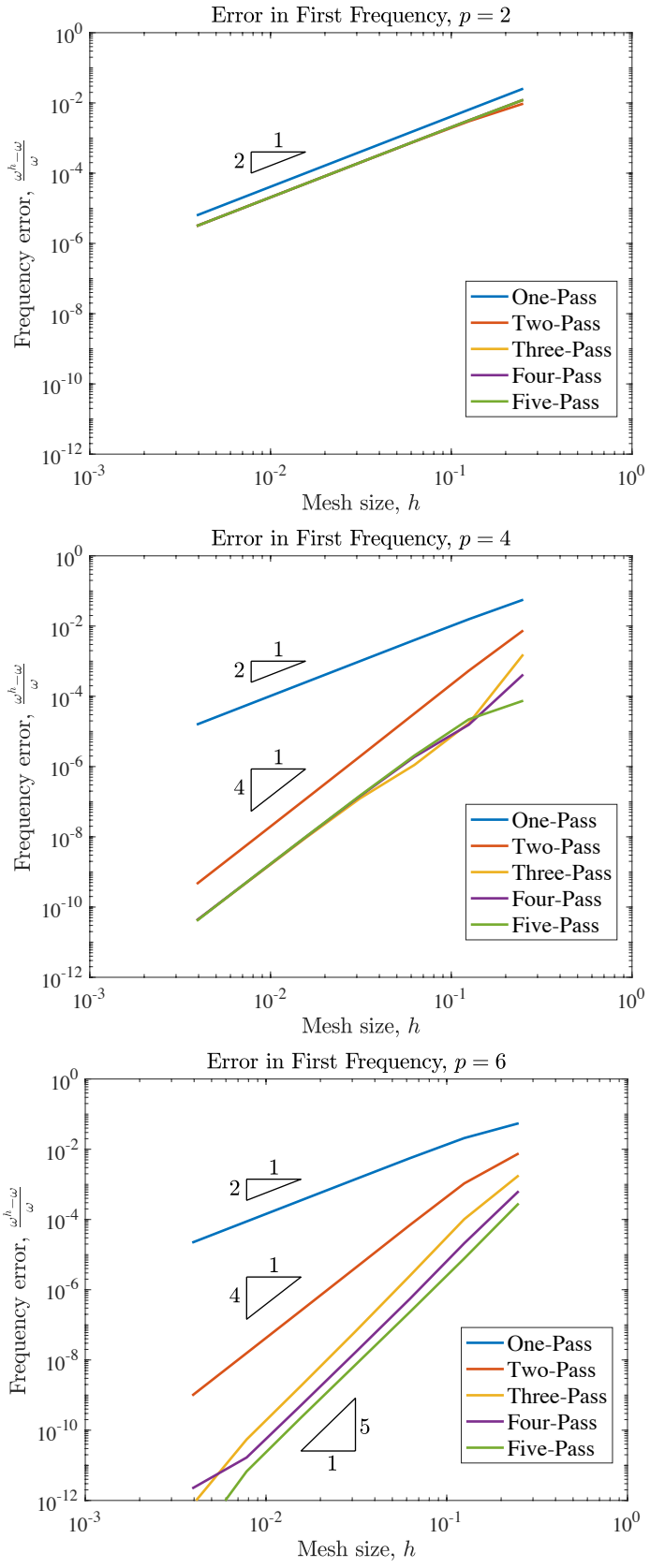

Figure 3: Errors in the first frequency versus mesh size for a 1D isogeometric collocation scheme as applied to a pure Dirichlet problem. Polynomial degrees $p = 2$ (top), $p = 4$ (middle), and $p = 6$ (bottom).

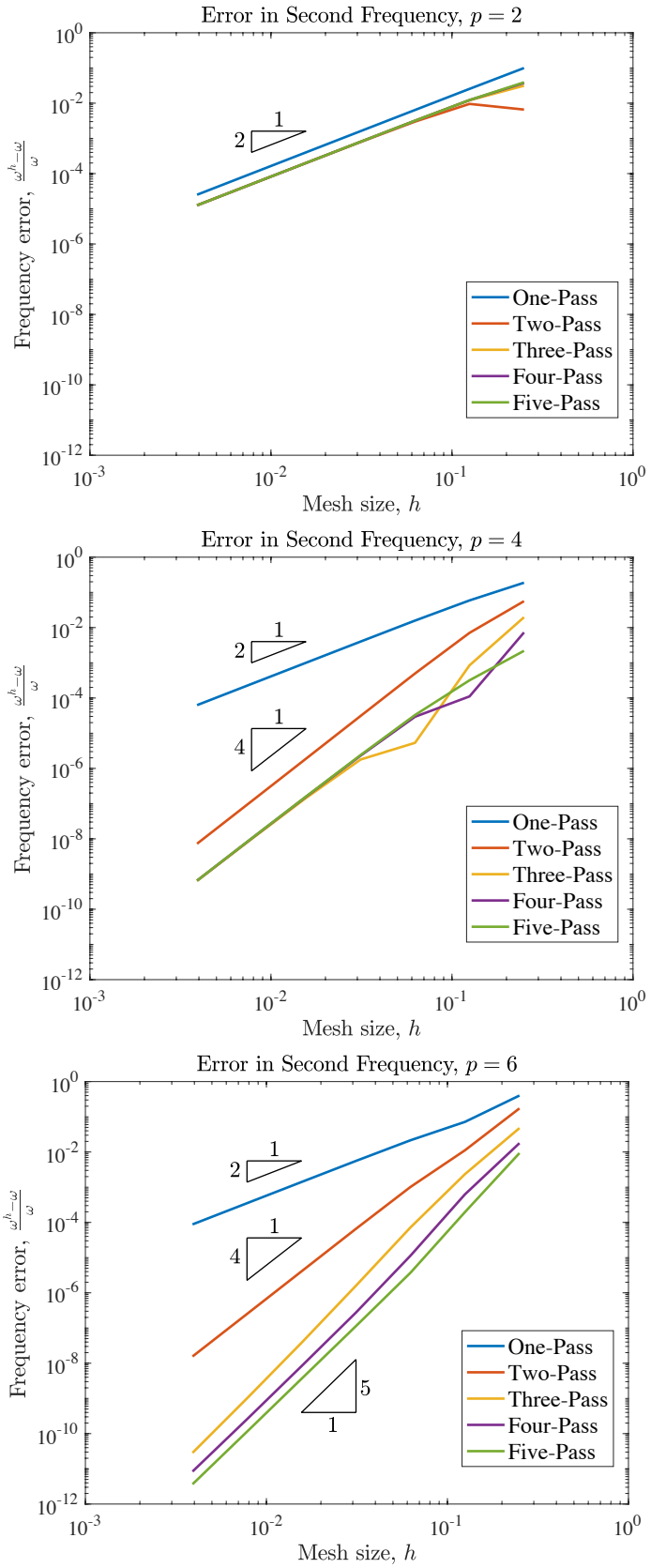

Figure 4: Errors in the second frequency versus mesh size for a 1D isogeometric collocation scheme as applied to a pure Dirichlet problem. Polynomial degrees $p = 2$ (top), $p = 4$ (middle), and $p = 6$ (bottom).

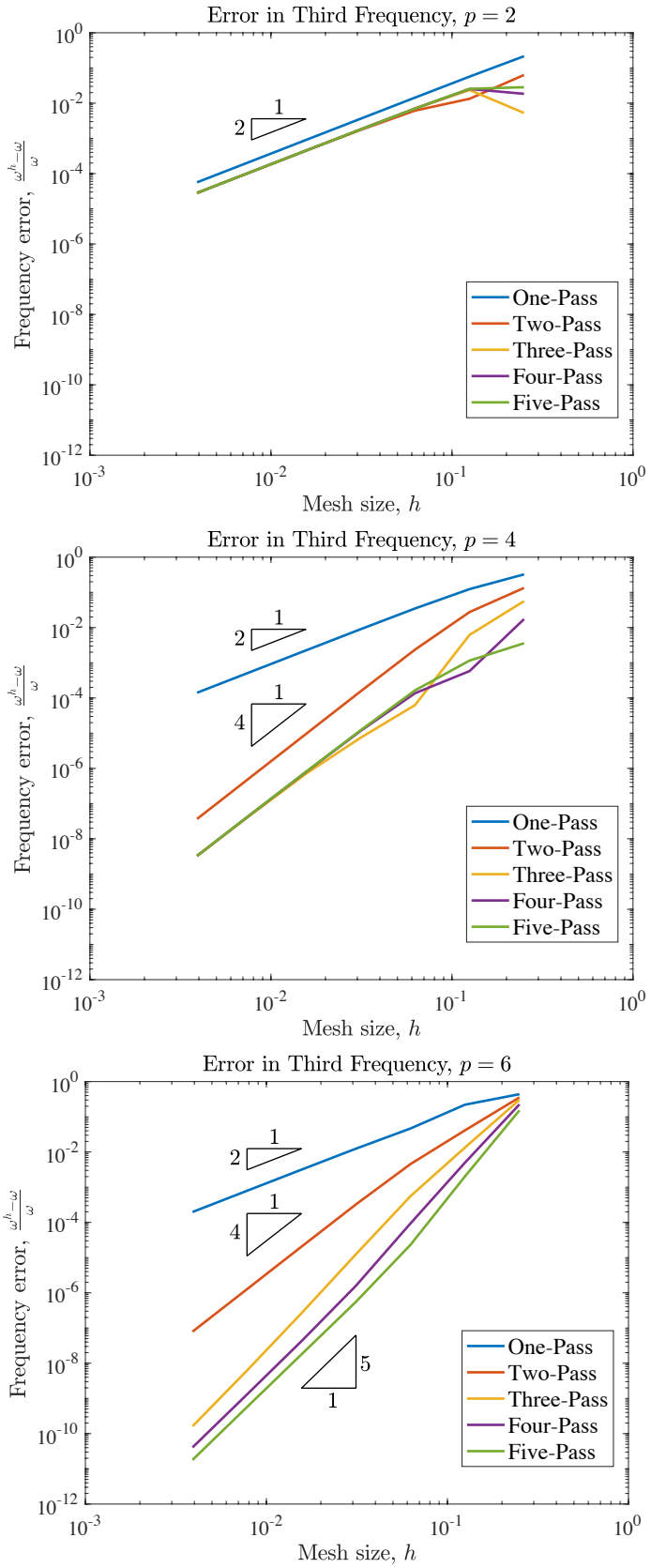

Figure 5: Errors in the third frequency versus mesh size for a 1D isogeometric collocation scheme as applied to a pure Dirichlet problem. Polynomial degrees $p = 2$ (top), $p = 4$ (middle), and $p = 6$ (bottom).

Neumann 1D eigenproblem: Find eigenvalues λ_n and eigenvectors u_n such that:

$$-\frac{d^2u_n}{dx^2} = \lambda_n u_n \tag{4.9}$$

in $\Omega = (0,1)$ subject to the boundary conditions $\frac{du_n}{dx}(0) = \frac{du_n}{dx}(1) = 0$. The exact solution to this problem is $(u_n(x), \lambda_n) = \left(\cos(n\pi x), (n\pi)^2\right)$ for $n = 0, 2, \ldots, \infty$. For all computations, we defined h^* to be the distance between the first two collocation points encountered from a Neumann collocation point. We also adopted a value of $C^* = 4$ as it has been found to yield optimal accuracy in prior work [15]. In Fig. 6(a), we have compared the discrete eigenfrequencies with the exact eigenfrequencies for $p = 2, 4, 6$ and $N = 1000$ when the consistent mass matrix has been employed, and in Fig. 6(b)-(f), we have compared the discrete eigenfrequencies with the exact eigenfrequencies for $p = 2, 4, 6$ and $N = 1000$ when the consistent mass matrix has been replaced with one through five passes of the predictor-multicorrector algorithm. We observe very similar behavior to that observed in the pure Dirichlet setting. In particular, the spectrum uniformly converges (with the exception of a finite number of outlier modes) with increasing polynomial degree when the consistent mass matrix is employed, and the spectrum uniformly improves with an increasing number of passes when the consistent mass matrix is replaced by a predictor-multicorrector algorithm.

As with the pure Dirichlet problem, we have also computed the errors of the first three eigenfrequencies resulting from the application of a 1D isogeometric collocation scheme to (4.9) where we have replaced the consistent mass matrix by a select number of passes of the predictor-multicorrector algorithm. In Fig. 7, we have reported errors in the first nonzero frequency versus mesh size for a 1D collocation collocation scheme for polynomial degrees $p = 2$, 4, and 6. From this figure, we observe that the eigenfrequency is second-order accurate for $p = 2$ no matter how many passes are conducted. For both $p = 4$ and $p = 6$, the eigenfrequency is second-order accurate if only one pass is conducted and third-order accurate if more than one pass is conducted. Unlike the pure Dirichlet problem, it appears that fourth-order accuracy is not possible using a fixed number of passes. In Fig. 8 and 9, we have reported errors in the second and third nonzero frequencies, respectively, versus mesh size for a 1D collocation collocation scheme for polynomial degrees $p = 2$, 4, and 6, and these results resemble those displayed in Fig. 7. However, we generally also observe higher-order pre-asymptotic rates for $p = 4$ and $p = 6$ if more than two passes are carried out. We have furthermore conducted a number of additional numerical experiments and have observed the following behavior in the frequency error:

$$\frac{\left|\omega_n^h - \omega_n\right|}{\omega_n} \approx \begin{cases} h^2 & \text{if } p = 2, 3 \text{ or } p > 3 \text{ with only one pass} \\ h^3 & \text{if } p > 3 \text{ with at least two passes} \end{cases} \tag{4.10}$$

and similar behavior in the eigenfunction error:

$$\frac{\left\|u_n^h - u_n\right\|_{L^2(\Omega)}}{\|u_n\|_{L^2(\Omega)}} \approx \begin{cases} h^2 & \text{if } p = 2, 3 \text{ or } p > 3 \text{ with only one pass} \\ h^3 & \text{if } p > 3 \text{ with at least two passes} \end{cases} \tag{4.11}$$

Consequently, we anticipate the following error estimate to hold for the semi-discrete predictor-multicorrector method as applied to the pure Neumann problem: For each $t \in (0, T)$, we have:

$$\frac{\left\|u^h(t) - u_n(t)\right\|_{L^2(\Omega)}}{|||u|||} \approx \begin{cases} h^2 & \text{if } p = 2, 3 \text{ or } p > 3 \text{ with only one pass} \\ h^3 & \text{if } p > 3 \text{ with at least two passes} \end{cases} \tag{4.12}$$

We have found that the above rates are independent of the constant C^*, and they also hold for mixed Dirichlet-Neumann problems. However, in general, we observe pre-asymptotic rates of $O(h^4)$ for both the frequency and eigenfunction error provided at least two passes are carried out. We have also examined the behavior of the semi-discrete multicorrector method for the pure Neumann problem when the Neumann

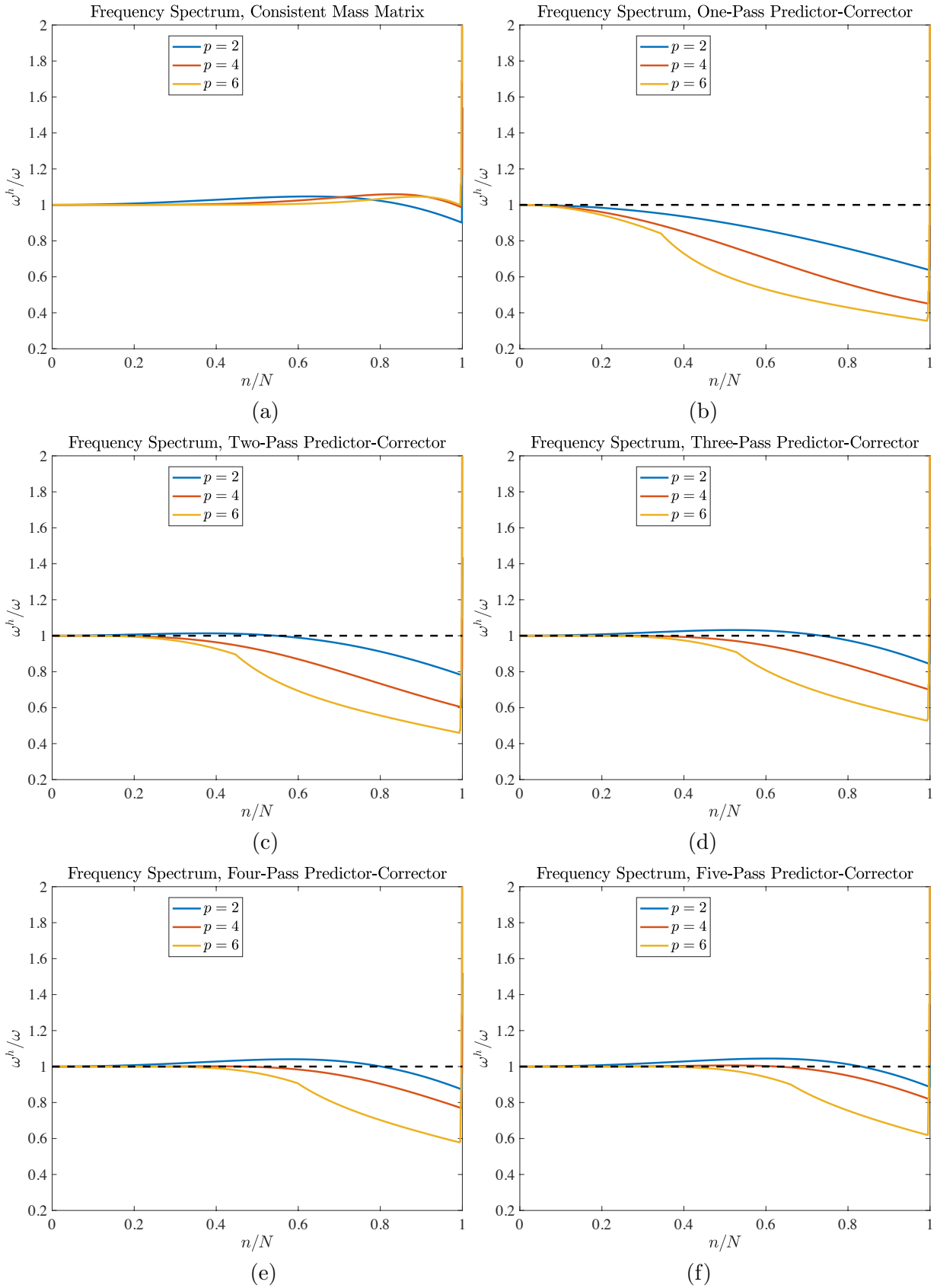

Figure 6: Eigenfrequency spectrum for a 1D isogeometric collocation scheme as applied to a pure Neumann problem when (a) the consistent mass matrix is employed, (b) one pass is employed in a predictor-multicorrector algorithm, (c) two passes are employed in a predictor-multicorrector algorithm, (d) three passes are employed in a predictor-multicorrector algorithm, (e) four passes are employed in a predictor-multicorrector algorithm, and (f) five passes are employed in a predictor-multicorrector algorithm. The dashed black lines in the above plots correspond to $\omega^h/\omega = 1$.

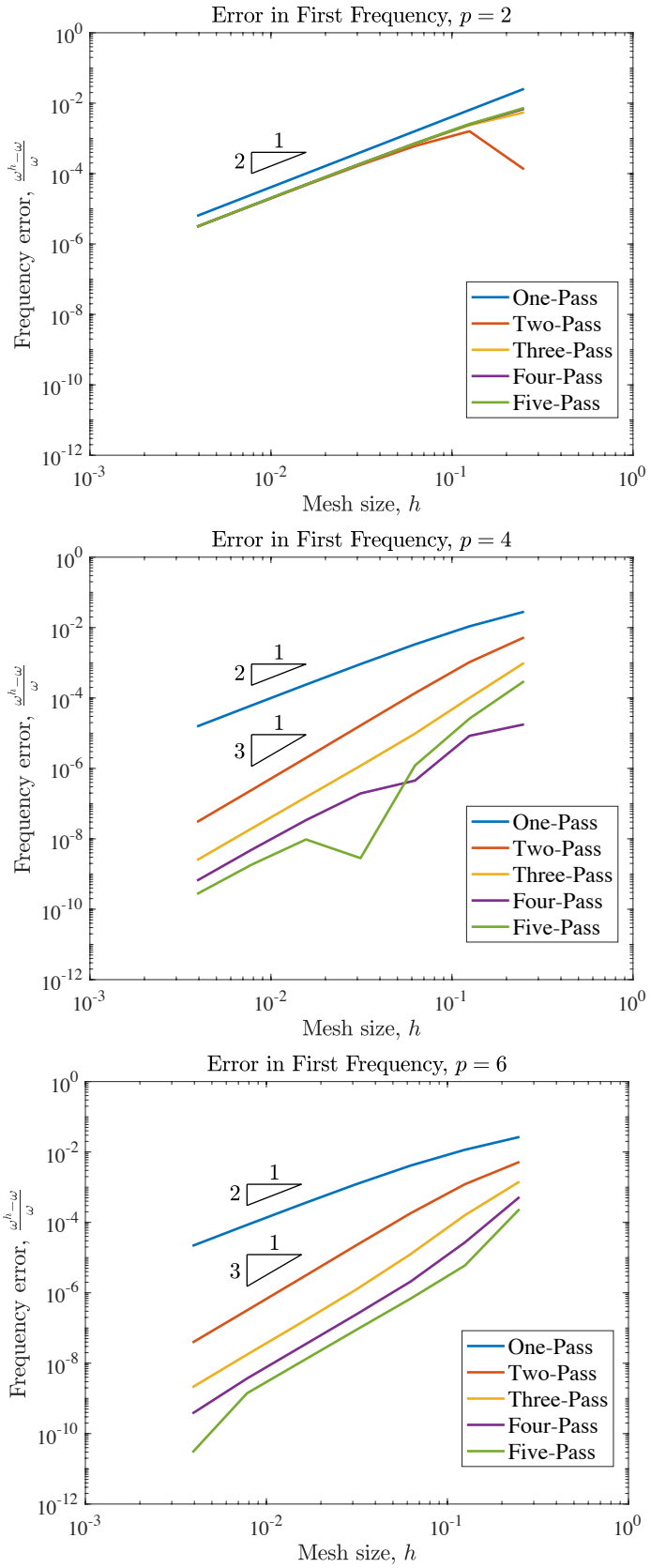

Figure 7: Errors in the first nonzero frequency versus mesh size for a 1D isogeometric collocation scheme as applied to a pure Neumann problem. Polynomial degrees $p = 2$ (top), $p = 4$ (middle), and $p = 6$ (bottom).

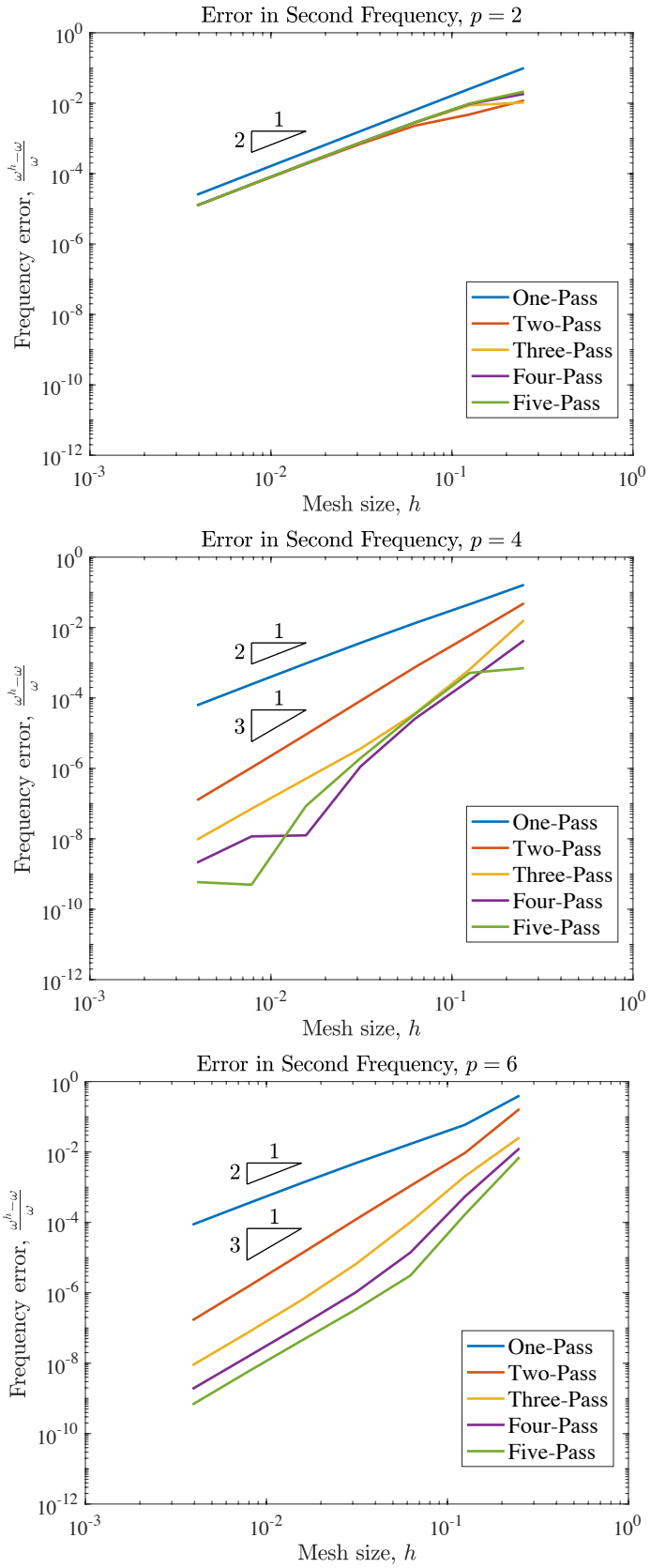

Figure 8: Errors in the second nonzero frequency versus mesh size for a 1D isogeometric collocation scheme as applied to a pure Neumann problem. Polynomial degrees $p = 2$ (top), $p = 4$ (middle), and $p = 6$ (bottom).

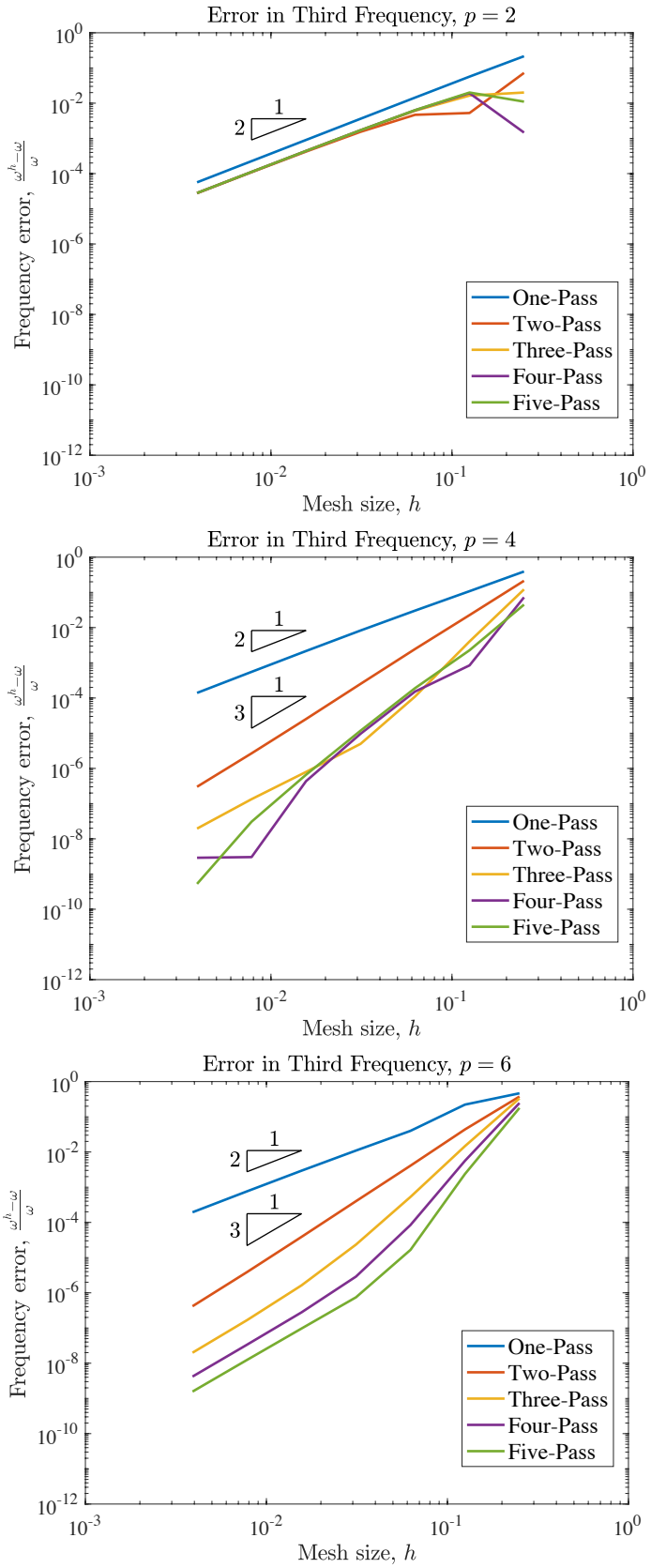

Figure 9: Errors in the third nonzero frequency versus mesh size for a 1D isogeometric collocation scheme as applied to a pure Neumann problem. Polynomial degrees $p = 2$ (top), $p = 4$ (middle), and $p = 6$ (bottom).

boundary conditions are applied in a standard manner (that is, the Neumann boundary conditions are collocated directly rather than in a weighted average with the governing partial differential equation). In this case, the eigenfrequencies were found to exhibit no better than first-order accuracy with a fixed number of passes, speaking to the importance of using the enhanced collocation method for Neumann boundary condition enforcement in the explicit dynamics setting.

5. Fully Discrete Explicit Predictor-Multicorrector Algorithms

We are now ready to present our family of fully discrete explicit isogeometric collocation methods. They result from the application of explicit time-integration schemes to the semi-discrete predictor-multicorrector system:

$$\mathsf{K}\overline{\mathbf{u}} + \mathsf{C}\overline{\mathbf{v}} + \mathsf{M}_r\overline{\mathbf{a}} = \mathsf{F} \tag{5.1}$$

where $\overline{\mathbf{v}} = \frac{d}{dt}\overline{\mathbf{u}}$ and $\overline{\mathbf{a}} = \frac{d^2}{dt^2}\overline{\mathbf{u}}$. Above, we have included the presence of a viscous damping matrix C for purposes of full generality. The classical Rayleigh damping matrix takes the form $\mathsf{C} = a\mathsf{M} + b\mathsf{K}$ where a and b are parameters selected to produce desired damping characteristics [21, Chapter 7]. We focus our attention on explicit Runge-Kutta methods given their widespread use in scientific and engineering practice. As explicit Runge-Kutta methods are specifically designed for first-order differential systems, we rewrite the semi-discrete predictor-multicorrector system as follows:

$$\frac{d}{dt}\mathbf{y}(t) = \mathbf{f}(\mathbf{y}, t) \tag{5.2}$$

where:

$$\mathbf{y}(t) = \begin{bmatrix} \mathbf{y}_1(t) \\ \mathbf{y}_2(t) \end{bmatrix} = \begin{bmatrix} \overline{\mathbf{u}}(t) \\ \overline{\mathbf{v}}(t) \end{bmatrix} \tag{5.3}$$

and:

$$\mathbf{f}(\mathbf{y}, t) = \begin{bmatrix} \mathbf{f}_1(\mathbf{y}, t) \\ \mathbf{f}_2(\mathbf{y}, t) \end{bmatrix} = \begin{bmatrix} \mathbf{y}_2(t) \\ \mathsf{M}_r^{-1}\left(\mathsf{F} - \mathsf{K}\mathbf{y}_1(t) - \mathsf{C}\mathbf{y}_2(t)\right) \end{bmatrix} \tag{5.4}$$

5.1. Second-Order-in-Time Explicit Predictor-Multicorrector Algorithm

The first explicit predictor-multicorrector algorithm we consider results from an application of the second-order Runge-Kutta method, also known as the explicit midpoint method, to the system given in (5.2). This yields the following algorithm for the displacement $\overline{\mathbf{u}}_{n+1}$ and velocity $\overline{\mathbf{v}}_{n+1}$ at time $t_{n+1} = (n+1)\Delta t$ given the displacement $\overline{\mathbf{u}}_n$ and velocity $\overline{\mathbf{v}}_n$ at time $t_n = n\Delta t$:

$$\text{(RK2)}\begin{cases} \hat{\mathbf{u}}_1 = \overline{\mathbf{u}}_n, \quad \hat{\mathbf{v}}_1 = \overline{\mathbf{v}}_n, \quad \hat{\mathbf{a}}_1 = \mathbf{0} \\ \text{for } i = 0, \ldots, r-1 \\ \qquad \Delta\hat{\mathbf{a}}_1 = (\mathsf{M}_L)^{-1}\left(\mathsf{F}_n - \mathsf{M}\hat{\mathbf{a}}_1 - \mathsf{K}\hat{\mathbf{u}}_1 - \mathsf{C}\hat{\mathbf{v}}_1\right), \quad \hat{\mathbf{a}}_1 = \hat{\mathbf{a}}_1 + \Delta\hat{\mathbf{a}}_1 \\ \text{end} \\ \hat{\mathbf{u}}_2 = \overline{\mathbf{u}}_n + \dfrac{\Delta t}{2}\hat{\mathbf{v}}_1, \quad \hat{\mathbf{v}}_2 = \overline{\mathbf{v}}_n + \dfrac{\Delta t}{2}\hat{\mathbf{a}}_1, \quad \hat{\mathbf{a}}_2 = \mathbf{0} \\ \text{for } i = 0, \ldots, r-1 \\ \qquad \Delta\hat{\mathbf{a}}_2 = (\mathsf{M}_L)^{-1}\left(\mathsf{F}_{n+1/2} - \mathsf{M}\hat{\mathbf{a}}_2 - \mathsf{K}\hat{\mathbf{u}}_2 - \mathsf{C}\hat{\mathbf{v}}_2\right), \quad \hat{\mathbf{a}}_2 = \hat{\mathbf{a}}_2 + \Delta\hat{\mathbf{a}}_2 \\ \text{end} \\ \overline{\mathbf{u}}_{n+1} = \overline{\mathbf{u}}_n + \Delta t\hat{\mathbf{v}}_2, \quad \overline{\mathbf{v}}_{n+1} = \overline{\mathbf{v}}_n + \Delta t\hat{\mathbf{a}}_2 \end{cases} \tag{5.5}$$

where the load vector $\mathsf{F}_{n+\alpha}$ is evaluated at time $t = (n+\alpha)\Delta t$ ($\alpha = 0, 1/2$). If needed, acceleration can be simply computed as $\overline{\mathbf{a}}_{n+1} = \mathsf{M}_r^{-1}(\mathsf{F}_{n+1} - \mathsf{K}\overline{\mathbf{u}}_{n+1})$.

5.2. Fourth-Order-in-Time Explicit Predictor-Multicorrector Algorithm

The next explicit predictor-multicorrector algorithm we consider results from an application of the fourth-order Runge-Kutta method, also known as the classical Runge-Kutta method [30], to the system given in (5.2). This yields the following algorithm for the n^{th} time-step:

$$
\text{(RK4)}\quad \left\{ \begin{array}{l}
\quad \hat{\mathbf{u}}_1 = \overline{\mathbf{u}}_n, \quad \hat{\mathbf{v}}_1 = \overline{\mathbf{v}}_n, \quad \hat{\mathbf{a}}_1 = \mathbf{0} \\
\text{for } i = 0, \ldots, r-1 \\
\qquad \Delta\hat{\mathbf{a}}_1 = (\mathsf{M}_L)^{-1} \left(\mathsf{F}_n - \mathsf{M}\hat{\mathbf{a}}_1 - \mathsf{K}\hat{\mathbf{u}}_1 - \mathsf{C}\hat{\mathbf{v}}_1 \right), \quad \hat{\mathbf{a}}_1 = \hat{\mathbf{a}}_1 + \Delta\hat{\mathbf{a}}_1 \\
\text{end} \\
\quad \hat{\mathbf{u}}_2 = \overline{\mathbf{u}}_n + \dfrac{\Delta t}{2}\hat{\mathbf{v}}_1, \quad \hat{\mathbf{v}}_2 = \overline{\mathbf{v}}_n + \dfrac{\Delta t}{2}\hat{\mathbf{a}}_1, \quad \hat{\mathbf{a}}_2 = \mathbf{0} \\
\text{for } i = 0, \ldots, r-1 \\
\qquad \Delta\hat{\mathbf{a}}_2 = (\mathsf{M}_L)^{-1} \left(\mathsf{F}_{n+1/2} - \mathsf{M}\hat{\mathbf{a}}_2 - \mathsf{K}\hat{\mathbf{u}}_2 - \mathsf{C}\hat{\mathbf{v}}_2 \right), \quad \hat{\mathbf{a}}_2 = \hat{\mathbf{a}}_2 + \Delta\hat{\mathbf{a}}_2 \\
\text{end} \\
\quad \hat{\mathbf{u}}_3 = \overline{\mathbf{u}}_n + \dfrac{\Delta t}{2}\hat{\mathbf{v}}_2, \quad \hat{\mathbf{v}}_3 = \overline{\mathbf{v}}_n + \dfrac{\Delta t}{2}\hat{\mathbf{a}}_2, \quad \hat{\mathbf{a}}_3 = \mathbf{0} \\
\text{for } i = 0, \ldots, r-1 \\
\qquad \Delta\hat{\mathbf{a}}_3 = (\mathsf{M}_L)^{-1} \left(\mathsf{F}_{n+1/2} - \mathsf{M}\hat{\mathbf{a}}_3 - \mathsf{K}\hat{\mathbf{u}}_3 - \mathsf{C}\hat{\mathbf{v}}_3 \right), \quad \hat{\mathbf{a}}_3 = \hat{\mathbf{a}}_3 + \Delta\hat{\mathbf{a}}_3 \\
\text{end} \\
\quad \hat{\mathbf{u}}_4 = \overline{\mathbf{u}}_n + \Delta t\hat{\mathbf{v}}_3, \quad \hat{\mathbf{v}}_4 = \overline{\mathbf{v}}_n + \Delta t\hat{\mathbf{a}}_3, \quad \hat{\mathbf{a}}_4 = \mathbf{0} \\
\text{for } i = 0, \ldots, r-1 \\
\qquad \Delta\hat{\mathbf{a}}_4 = (\mathsf{M}_L)^{-1} \left(\mathsf{F}_{n+1} - \mathsf{M}\hat{\mathbf{a}}_4 - \mathsf{K}\hat{\mathbf{u}}_4 - \mathsf{C}\hat{\mathbf{v}}_4 \right), \quad \hat{\mathbf{a}}_4 = \hat{\mathbf{a}}_4 + \Delta\hat{\mathbf{a}}_4 \\
\text{end} \\
\overline{\mathbf{u}}_{n+1} = \overline{\mathbf{u}}_n + \dfrac{\Delta t}{6} \left(\hat{\mathbf{v}}_1 + 2\hat{\mathbf{v}}_2 + 2\hat{\mathbf{v}}_3 + \hat{\mathbf{v}}_4 \right) \\
\overline{\mathbf{v}}_{n+1} = \overline{\mathbf{v}}_n + \dfrac{\Delta t}{6} \left(\hat{\mathbf{a}}_1 + 2\hat{\mathbf{a}}_2 + 2\hat{\mathbf{a}}_3 + \hat{\mathbf{a}}_4 \right)
\end{array} \right. \tag{5.6}
$$

It is important to note that the corrector phase involves four corrector "for loops", so a single corrector pass has a cost two times higher than the corrector phase of the previous algorithm.

5.3. Fifth-Order-in-Time Explicit Predictor-Multicorrector Algorithm

The last explicit predictor-multicorrector algorithm we consider results from an application of Butcher's fifth-order Runge-Kutta method, which consists of six stages [9]. Application of Butcher's method yields the following algorithm for the n^{th} time-step:

$$
\text{(RK5)}\quad \left\{
\begin{array}{l}
\hat{\mathbf{u}}_1 = \overline{\mathbf{u}}_n, \quad \hat{\mathbf{v}}_1 = \overline{\mathbf{v}}_n, \quad \hat{\mathbf{a}}_1 = \mathbf{0} \\
\text{for } i = 0, \ldots, r-1 \\
\qquad \Delta\hat{\mathbf{a}}_1 = (\mathsf{M}_L)^{-1} \left(\mathsf{F}_n - \mathsf{M}\hat{\mathbf{a}}_1 - \mathsf{K}\hat{\mathbf{u}}_1 - \mathsf{C}\hat{\mathbf{v}}_1\right), \quad \hat{\mathbf{a}}_1 = \hat{\mathbf{a}}_1 + \Delta\hat{\mathbf{a}}_1 \\
\text{end} \\
\hat{\mathbf{u}}_2 = \overline{\mathbf{u}}_n + \dfrac{\Delta t}{4}\hat{\mathbf{v}}_1, \quad \hat{\mathbf{v}}_2 = \overline{\mathbf{v}}_n + \dfrac{\Delta t}{4}\hat{\mathbf{a}}_1, \quad \hat{\mathbf{a}}_2 = \mathbf{0} \\
\text{for } i = 0, \ldots, r-1 \\
\qquad \Delta\hat{\mathbf{a}}_2 = (\mathsf{M}_L)^{-1} \left(\mathsf{F}_{n+1/4} - \mathsf{M}\hat{\mathbf{a}}_2 - \mathsf{K}\hat{\mathbf{u}}_2 - \mathsf{C}\hat{\mathbf{v}}_2\right), \quad \hat{\mathbf{a}}_2 = \hat{\mathbf{a}}_2 + \Delta\hat{\mathbf{a}}_2 \\
\text{end} \\
\hat{\mathbf{u}}_3 = \overline{\mathbf{u}}_n + \dfrac{\Delta t}{8}\left(\hat{\mathbf{v}}_1 + \hat{\mathbf{v}}_2\right), \quad \hat{\mathbf{v}}_3 = \overline{\mathbf{v}}_n + \dfrac{\Delta t}{8}\left(\hat{\mathbf{a}}_1 + \hat{\mathbf{a}}_2\right), \quad \hat{\mathbf{a}}_3 = \mathbf{0} \\
\text{for } i = 0, \ldots, r-1 \\
\qquad \Delta\hat{\mathbf{a}}_3 = (\mathsf{M}_L)^{-1} \left(\mathsf{F}_{n+1/4} - \mathsf{M}\hat{\mathbf{a}}_3 - \mathsf{K}\hat{\mathbf{u}}_3 - \mathsf{C}\hat{\mathbf{v}}_3\right), \quad \hat{\mathbf{a}}_3 = \hat{\mathbf{a}}_3 + \Delta\hat{\mathbf{a}}_3 \\
\text{end} \\
\hat{\mathbf{u}}_4 = \overline{\mathbf{u}}_n + \dfrac{\Delta t}{2}\left(-\hat{\mathbf{v}}_2 + 2\hat{\mathbf{v}}_3\right), \quad \hat{\mathbf{v}}_4 = \overline{\mathbf{v}}_n + \dfrac{\Delta t}{2}\left(-\hat{\mathbf{a}}_2 + 2\hat{\mathbf{a}}_3\right), \quad \hat{\mathbf{a}}_4 = \mathbf{0} \\
\text{for } i = 0, \ldots, r-1 \\
\qquad \Delta\hat{\mathbf{a}}_4 = (\mathsf{M}_L)^{-1} \left(\mathsf{F}_{n+1/2} - \mathsf{M}\hat{\mathbf{a}}_4 - \mathsf{K}\hat{\mathbf{u}}_4 - \mathsf{C}\hat{\mathbf{v}}_4\right), \quad \hat{\mathbf{a}}_4 = \hat{\mathbf{a}}_4 + \Delta\hat{\mathbf{a}}_4 \\
\text{end} \\
\hat{\mathbf{u}}_5 = \overline{\mathbf{u}}_n + \dfrac{\Delta t}{16}\left(3\hat{\mathbf{v}}_1 + 9\hat{\mathbf{v}}_4\right), \quad \hat{\mathbf{v}}_5 = \overline{\mathbf{v}}_n + \dfrac{\Delta t}{16}\left(3\hat{\mathbf{a}}_1 + 9\hat{\mathbf{a}}_4\right), \quad \hat{\mathbf{a}}_5 = \mathbf{0} \\
\text{for } i = 0, \ldots, r-1 \\
\qquad \Delta\hat{\mathbf{a}}_5 = (\mathsf{M}_L)^{-1} \left(\mathsf{F}_{n+3/4} - \mathsf{M}\hat{\mathbf{a}}_5 - \mathsf{K}\hat{\mathbf{u}}_5 - \mathsf{C}\hat{\mathbf{v}}_5\right), \quad \hat{\mathbf{a}}_5 = \hat{\mathbf{a}}_5 + \Delta\hat{\mathbf{a}}_5 \\
\text{end} \\
\hat{\mathbf{u}}_6 = \overline{\mathbf{u}}_n + \dfrac{\Delta t}{7}\left(-3\hat{\mathbf{v}}_1 + 2\hat{\mathbf{v}}_2 + 12\hat{\mathbf{v}}_3 - 12\hat{\mathbf{v}}_4 + 8\hat{\mathbf{v}}_5\right) \\
\hat{\mathbf{v}}_6 = \overline{\mathbf{v}}_n + \dfrac{\Delta t}{7}\left(-3\hat{\mathbf{a}}_1 + 2\hat{\mathbf{a}}_2 + 12\hat{\mathbf{a}}_3 - 12\hat{\mathbf{a}}_4 + 8\hat{\mathbf{a}}_5\right) \\
\hat{\mathbf{a}}_6 = \mathbf{0} \\
\text{for } i = 0, \ldots, r-1 \\
\qquad \Delta\hat{\mathbf{a}}_6 = (\mathsf{M}_L)^{-1} \left(\mathsf{F}_{n+1} - \mathsf{M}\hat{\mathbf{a}}_6 - \mathsf{K}\hat{\mathbf{u}}_6 - \mathsf{C}\hat{\mathbf{v}}_6\right), \quad \hat{\mathbf{a}}_6 = \hat{\mathbf{a}}_6 + \Delta\hat{\mathbf{a}}_6 \\
\text{end} \\
\overline{\mathbf{u}}_{n+1} = \overline{\mathbf{u}}_n + \dfrac{\Delta t}{90}\left(7\hat{\mathbf{v}}_1 + 32\hat{\mathbf{v}}_3 + 12\hat{\mathbf{v}}_4 + 32\hat{\mathbf{v}}_5 + 7\hat{\mathbf{v}}_6\right) \\
\overline{\mathbf{v}}_{n+1} = \overline{\mathbf{v}}_n + \dfrac{\Delta t}{90}\left(7\hat{\mathbf{a}}_1 + 32\hat{\mathbf{a}}_3 + 12\hat{\mathbf{a}}_4 + 32\hat{\mathbf{a}}_5 + 7\hat{\mathbf{a}}_6\right)
\end{array}
\right. \tag{5.7}
$$

The corrector phase involves six corrector "for loops", so a single corrector pass has a cost three times higher than the corrector phase of the second-order algorithm and one and a half times higher than the corrector phase of the fourth-order algorithm.

6. Assessment of Computational Cost

We assess the computational cost associated with our family of explicit isogeometric collocation methods. To conduct such an assessment, we first identify the maximum stable time-step size for each of the

presented methods and then determine the corresponding computational cost per time step. We conclude this section with a short discussion on parallel implementation.

6.1. Critical Time-Step Size

We begin our assessment of computational cost by computing the critical time-step size associated with the fully discrete predictor-multicorrector algorithms presented in Section 5. It is well-known that the maximum stable time-step size associated with explicit time integration of a linear system of ordinary differential equations of the form (3.8) is equal to:

$$\Delta t_{\max} = \frac{C_{\max}}{\omega^h_{\max}} \tag{6.1}$$

where $\omega^h_{\max}$ is the maximum eigenfrequency associated with the eigenproblem (4.1) and $C_{\max}$ is a positive constant related to the chosen time integration routine [21, Chapter 9]. For the second-order, fourth-order, and fifth-order Runge-Kutta methods considered in this work, $C_{\max} = 2.000$, 2.785, and 3.387 respectively [34]. We have tabulated the maximum frequency $\omega^h_{\max}$ multiplied by the mesh size h for the 1D case with Dirichlet boundary conditions and a range of polynomial degrees and corrector passes in Table 2. To arrive at the reported values, we computed the maximum frequencies associated with $N = 1000$. We observe that the maximum frequency increases with the number of corrector passes, which is consistent with what was observed in Figure 2. Moreover, we observe that the maximum frequency increases at roughly a linear rate with the polynomial degree. This is due to the presence of outlier modes in the discrete system. We also have tabulated in Table 3 the critical time-step size $\Delta t_{\max}$ normalized by the mesh size h for the 1D case with Dirichlet boundary conditions and the explicit isogeometric methods presented in Section 5. Recalling that one, two, and three corrector passes are required for second-order-in-space, fourth-order-in-space, and fifth-order-in-space accuracy respectively, we see that the critical time-step size is between $0.5h$ and h when a minimal number of passes to guarantee optimal convergence is employed. This is quite favorable especially in comparison with explicit finite element [21], spectral element [31], and discontinuous Galerkin [29] methodologies.

To examine the impact of alternative sets of boundary conditions, we have also tabulated the maximum frequency $\omega^h_{\max}$ multiplied by the mesh size h for the 1D case with Neumann boundary conditions and a range of polynomial degrees and corrector passes in Table 4. For all computations, we computed the maximum frequencies associated with $N = 1000$. We also defined h^* to be the distance between the first two collocation points encountered from a Neumann collocation point, and we selected $C^* = 4$. From the table, we observe that the maximum frequency increases with the number of corrector passes and with the polynomial degree as in the setting of Dirichlet boundary conditions. Moreover, the maximum frequencies associated with the Neumann problem are larger than the maximum frequencies associated with the Dirichlet problem, though they are still quite favorable in comparison with explicit finite element, spectral element, and discontinuous Galerkin methodologies. We have also observed that the maximum frequency increases with increasing C^*. The maximum frequencies associated with the Neumann problem coincide with those of the Dirichlet problem when $C^* = 1$. However, the discrete eigenfrequencies are complex-valued in this case, so the corresponding discrete solutions are highly unstable. In the limit as $C^* \to \infty$, the maximum frequency tends to infinity. This coincides with the fact that our system of

Table 2: Maximum frequency $\omega^h_{\max}$ multiplied by the mesh size h for the 1D case with Dirichlet BCs.

Polynomial Degree/Corrector Passes	$r = 1$	$r = 2$	$r = 3$
$p = 2$	2.000	2.450	2.646
$p = 4$	3.018	3.748	4.136
$p = 6$	4.310	5.350	5.903

Table 3: Critical time-step size $\Delta t_{\max}$ normalized by the mesh size h for the 1D case with Dirichlet BCs.

RK2 Predictor-Multicorrector Algorithm

Polynomial Degree/Corrector Passes	$r = 1$	$r = 2$	$r = 3$
$p = 2$	1.000	0.816	0.756
$p = 4$	0.663	0.534	0.484
$p = 6$	0.464	0.374	0.339

RK4 Predictor-Multicorrector Algorithm

Polynomial Degree/Corrector Passes	$r = 1$	$r = 2$	$r = 3$
$p = 2$	1.393	1.137	1.053
$p = 4$	0.923	0.743	0.673
$p = 6$	0.646	0.521	0.472

RK5 Predictor-Multicorrector Algorithm

Polynomial Degree/Corrector Passes	$r = 1$	$r = 2$	$r = 3$
$p = 2$	1.693	1.382	1.280
$p = 4$	1.122	0.904	0.819
$p = 6$	0.786	0.633	0.574

Table 4: Maximum frequency $\omega^h_{\max}$ multiplied by the mesh size h for the 1D case with Neumann BCs.

Polynomial Degree/Corrector Passes	$r = 1$	$r = 2$	$r = 3$
$p = 2$	4.000	4.511	4.699
$p = 4$	7.638	8.746	9.207
$p = 6$	11.28	12.97	13.68

ordinary differential equations transforms into a system of differential-algebraic equations when Neumann boundary conditions are imposed using a standard collocation treatment.

6.2. Computational Cost per Time-Step

Now that we have identified the critical time-step size associated with several members of our family of explicit isogeometric methods, we next quantify the computational cost associated with a single time step. To do so, we have counted every single floating point operation (FLOP) associated with the second-order-in-time, fourth-order-in-time, and fifth-order-in-time predictor-multicorrector algorithms presented in Section 5 and collected the results in Table 5. It should be noted that every assignment, addition, multiplication, and multiply-then-accumulate operation was assumed to consist of one FLOP in our counting, and one evaluation of a component of the applied forcing was also assumed to consist of one FLOP. Moreover, it was assumed that the system mass, stiffness, and damping matrices were pre-computed, though these matrices can be very efficiently constructed using $O\left((p+1)^d\right)$ operations per-degrees-of-freedom in the isogeometric collocation setting [39]. It should be mentioned that the reported counts are associated with interior degrees of freedom, and lower counts are associated with boundary degrees of freedom.

From Table 5, we see that the computational cost per-degree-of-freedom (per DOF) for our family of explicit isogeometric methods is quite low. In fact, it is nearly comparable to that of explicit finite-difference time-domain methods. The relative advantage of the explicit finite-difference time-domain approach is that one does not need to turn to the use of predictor-multicorrector schemes for system solution as the mass matrix is diagonal by construction. Consequently, our methods are roughly r times

Table 5: Floating point operations per-degree-of-freedom for a given time-step.

Algorithm	FLOPs per DOF
RK2 Predictor-Multicorrector Algorithm	$2(r+2d)(p+1)^d + 4r + 14$
RK4 Predictor-Multicorrector Algorithm	$4(r+2d)(p+1)^d + 8r + 31$
RK5 Predictor-Multicorrector Algorithm	$6(r+2d)(p+1)^d + 12r + 45$

more expensive than explicit finite-difference time-domain methods of comparable accuracy. For instance, our fourth-order-in-time predictor-multicorrector algorithm with $p = 4$ and $r = 2$ exhibits a cost of 4,047 FLOPs per DOF at each time-step in the three-dimensional setting, while the standard fourth-order finite-difference time-domain method [40] exhibits a cost of 3,047 FLOPs per DOF at each time-step. However, the increase in cost of an explicit isogeometric collocation method is offset by ease of implementation in the complex geometry setting in comparison with the finite-difference time-domain method.

6.3. Parallel Implementation

We conclude this section with a short discussion of parallel implementation. Every step in each of the explicit predictor-multicorrector algorithms is trivially parallelizable except for the matrix-vector products. However, as the matrices involved in said matrix-vector products are highly sparse, one can appeal to ghost regions to reliably and scalably communicate data between processes in a parallel matrix-vector product implementation. Such regions are easily implemented in parallel scientific computing packages such as PETSc [6] and Trilinos [19].

7. Numerical Results

In this section, we present a suite of numerical examples which confirm the accuracy of our family of explicit isogeometric collocation methods. In particular, we consider the following example problems:

i) Dynamics of a clamped-clamped rod, excited by an initial velocity distribution;
ii) Dynamics of a clamped-free rod, excited by an initial velocity distribution;
iii) Dynamics of a clamped plane-strain quarter annulus, excited by a time-dependent body force and an initial velocity distribution; and
iv) Dynamics of an elastic block, excited by a time-dependent body force, an initial velocity distribution, and prescribed Dirichlet boundary conditions.

Unless otherwise specified, we choose a time-step equal to $\Delta t = h/10$ where h is the greatest distance between adjacent collocation points, and we select the spatial and temporal discretizations as to match the spatial and temporal rates of convergence.. This yields a stable method for all considered cases (the critical time-step size $\Delta t_{\max}$ is approximately $h/6$ in the worst case corresponding to $p = 6$, $r = 5$, and Neumann boundary conditions), and it ensures that the error due to time discretization is comparable to the error due to spatial discretization as well as the error due to the number of passes employed in the predictor-multicorrector method. We employ uniform meshes for each example. We establish initial conditions using the same predictor-multicorrector method as in our explicit time-integration scheme. More specifically, we solve the collocated initial displacement and velocity equations given (2.10) and (2.11) by using the predictor-multicorrector algorithm provided in Section 3 with the same number of passes as employed in the explicit time-integration scheme itself. In the presence of Neumann boundary conditions, we define h^* to be the distance between the first two collocation points encountered from a Neumann collocation point, and we select $C^* = 4$. Damping is not considered in any of the presented numerical examples, though similar results have been obtained when damping is present.

7.1. Dynamics of a Clamped-Clamped Rod

We first consider a 1D elastodynamics problem governing the dynamics of a clamped-clamped rod occupying the domain $\Omega = (0, 1)$ excited by an initial velocity distribution. The governing equation for this problem is:

$$\ddot{u}(x,t) - \frac{\partial^2 u}{\partial x^2}(x,t) = 0 \qquad \forall x \in \Omega, t \in (0,T) \tag{7.1}$$

where $u = u(x,t)$ is the unknown displacement, a function of the axial coordinate x and time t respectively, and the boundary conditions for this problem are:

$$u(0,t) = u(1,t) = 0 \quad \forall t \in (0,T) \tag{7.2}$$

We consider the following initial conditions:

$$u(x,0) = 0, \quad \dot{u}(x,0) = 2\pi \sin(2\pi x) \quad \forall x \in \Omega \tag{7.3}$$

such that the exact solution is:

$$u(x,t) = \sin(2\pi x)\sin(2\pi t) \tag{7.4}$$

We have solved this problem using a variety of explicit isogeometric collocation methods and a sequence of meshes consisting of 5 through 160 elements[4] up to a final time of $T = 1.925$. In Fig. 10(a), we plot the L^2-error in the displacement field at time $t = T$ as a function of h for $p = 2$ and the second-order Runge-Kutta method for both the case when the consistent mass matrix is employed as well as when it is replaced by one through five passes of the predictor-multicorrector algorithm. Note that the displacement field is second-order accurate no matter how many passes are conducted. Moreover, provided that at least two corrector passes are carried out, the consistent mass matrix and predictor-multi-corrector results are indistinguishable. In Fig. 10(b), we plot the L^2-error in the strain field at time $t = T$ as a function of h for $p = 2$ and the second-order Runge-Kutta method. The strain field is second-order accurate no matter how many passes are conducted, and again the consistent mass matrix and predictor-multicorrector results are indistinguishable if two or more corrector passes are carried out. In Fig. 10(c) and (d), we plot the L^2-error in the displacement and strain fields respectively at time $t = T$ as a function of h for $p = 4$ and the fourth-order Runge-Kutta method. If one corrector pass is carried out, the displacement and strain fields are second-order accurate, while if two or more corrector passes are carried out, the displacement and strain fields are both fourth-order accurate. If three or more corrector passes are carried out, the consistent mass matrix and predictor-multicorrector results are nearly indistinguishable. In Fig. 10(e) and (f), we plot the L^2-error in the displacement and strain fields respectively at time $t = T$ as a function of h for $p = 6$ and the fifth-order Runge-Kutta method. As expected, the predictor-multicorrector method underperforms an explicit isogeometric collocation method using a consistent mass matrix for this case. If one corrector pass is carried out, the displacement and strain fields are second-order accurate. If two corrector passes are carried out, the displacement and strain fields are fourth-order accurate. If three or more corrector passes are carried out, the displacement field is fifth-order accurate, while the strain field is pre-asymptotically fifth-order accurate but only asymptotically fourth-order accurate. We have conducted a large number of additional studies, and we found that it was not possible to obtain higher than fifth-order accurate displacement fields and fourth-order accurate strain fields using a fixed number of corrector steps. Surprisingly, the displacement and strain fields are both sixth-order accurate for $p = 6$ when the consistent mass matrix is employed even though a fifth-order-in-time explicit time-integration scheme is utilized.

[4] In the context of isogeometric collocation, an element corresponds to a cell in the mesh formed by the knot vector in the 1D setting and the tensor-product of knot vectors in the 2D and 3D settings. This is the same as a Bézier element in the usual lingo of Isogeometric Analysis [8].

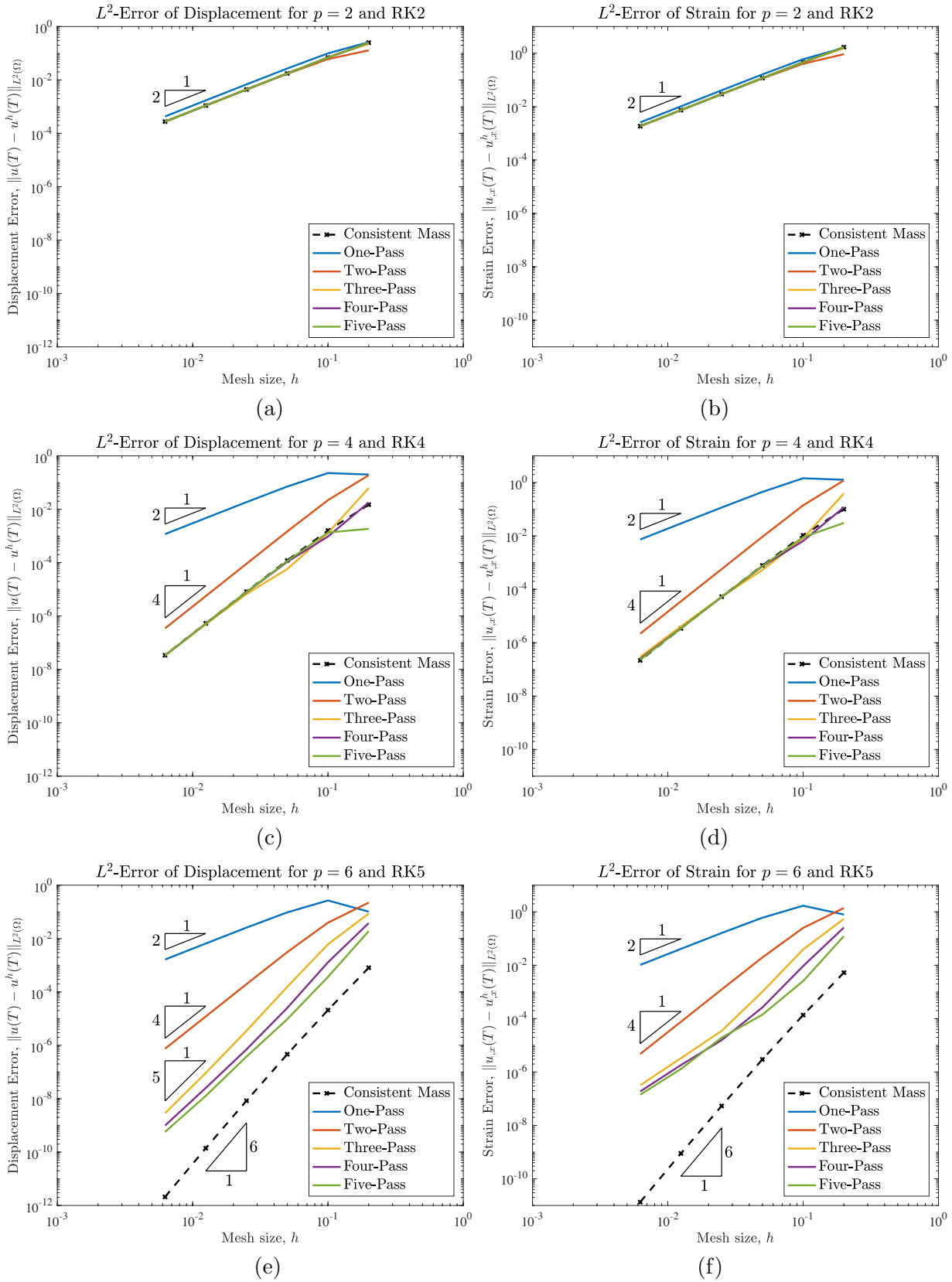

Figure 10: Convergence of explicit isogeometric collocation methods as applied to the clamped-clamped rod problem. (a) Convergence of displacement for $p = 2$. (b) Convergence of strain for $p = 2$. (c) Convergence of displacement for $p = 4$. (d) Convergence of strain for $p = 4$. (e) Convergence of displacement for $p = 6$. (f) Convergence of strain for $p = 6$.

7.2. Dynamics of a Clamped-Free Rod

We next consider a 1D elastodynamics problem governing the dynamics of a clamped-free rod occupying the domain $\Omega = (0, 1)$ excited by an initial velocity distribution. The governing equation for this problem is again:

$$\ddot{u}(x,t) - \frac{\partial^2 u}{\partial x^2}(x,t) = 0 \qquad \forall x \in \Omega, t \in (0,T) \tag{7.5}$$

and the boundary conditions for this problem are:

$$u(0,t) = \frac{\partial u}{\partial x}(1,t) = 0 \quad \forall t \in (0,T) \tag{7.6}$$

We consider the following initial conditions:

$$u(x,0) = 0, \quad \dot{u}(x,0) = \frac{5\pi}{2} \sin\left(\frac{5\pi}{2}\pi x\right) \quad \forall x \in \Omega \tag{7.7}$$

such that the exact solution is:

$$u(x,t) = \sin\left(\frac{5\pi}{2}x\right) \sin\left(\frac{5\pi}{2}t\right) \tag{7.8}$$

As with the clamped-clamped rod problem, we have solved this problem using a variety of explicit isogeometric collocation methods and a sequence of meshes consisting of 5 through 160 elements up to a final time of $T = 1.925$. In Fig. 11(a), we plot the L^2-error in the displacement field at time $t = T$ as a function of h for $p = 2$ and the second-order Runge-Kutta method for both the case when the consistent mass matrix is employed as well as when it is replaced by one through five passes of the predictor-multicorrector algorithm. Note that the displacement field is second-order accurate no matter how many passes are conducted, and provided that at least two corrector passes are carried out, the consistent mass matrix and predictor-multi-corrector results are indistinguishable. In Fig. 11(b), we plot the L^2-error in the strain field at time $t = T$ as a function of h for $p = 2$ and the second-order Runge-Kutta method. Like the displacement field, the strain field is second-order accurate no matter how many passes are conducted, and the consistent mass matrix and predictor-multicorrector results are indistinguishable if two or more corrector passes are carried out. In Fig. 11(c) and (d), we plot the L^2-error in the displacement and strain fields respectively at time $t = T$ as a function of h for $p = 4$ and the fourth-order Runge-Kutta method. If one corrector pass is carried out, the displacement and strain fields are second-order accurate. If two corrector passes are carried out, the displacement and strain fields are third-order accurate. If three or more corrector passes are carried out, the displacement field seems to exhibit fourth-order accuracy, and the consistent mass matrix and predictor-multicorrector displacement results are indistinguishable. This indicates improvement over our results from Section 4. However, we have confirmed that this is simply pre-asymptotic convergence behavior (though asymptotic behavior is not seen until more than 512 elements are employed), and the displacement field exhibits third-order accuracy at high levels of mesh resolution. Moreover, if three or more corrector passes are carried out, the strain field is also pre-asymptotically fourth-order accurate and asymptotically third-order accurate.

7.3. Dynamics of a Clamped Plane-Strain Quarter Annulus

We now consider a 2D elastodynamics problem on a non-square geometry, namely the dynamics of a clamped plane-strain quarter annulus excited by a time-dependent body force and an initial velocity distribution. The problem is graphically depicted in Fig. 12, and the annulus is chosen to have radii $R_1 = 1$ and $R_2 = 4$, density $\rho = 1.0$, and Lamé constants of $\mu = \lambda = 1.0$. The body force and velocity distribution are chosen such that the exact solution is

$$\begin{cases} u_1 = (x_1^2 + x_2^2 - 1)(x_1^2 + x_2^2 - 16)\sin(x_1)\sin(x_2)\sin(2\pi t), \\ u_2 = (x_1^2 + x_2^2 - 1)(x_1^2 + x_2^2 - 16)\sin(x_1)\sin(x_2)\sin(2\pi t). \end{cases} \tag{7.9}$$

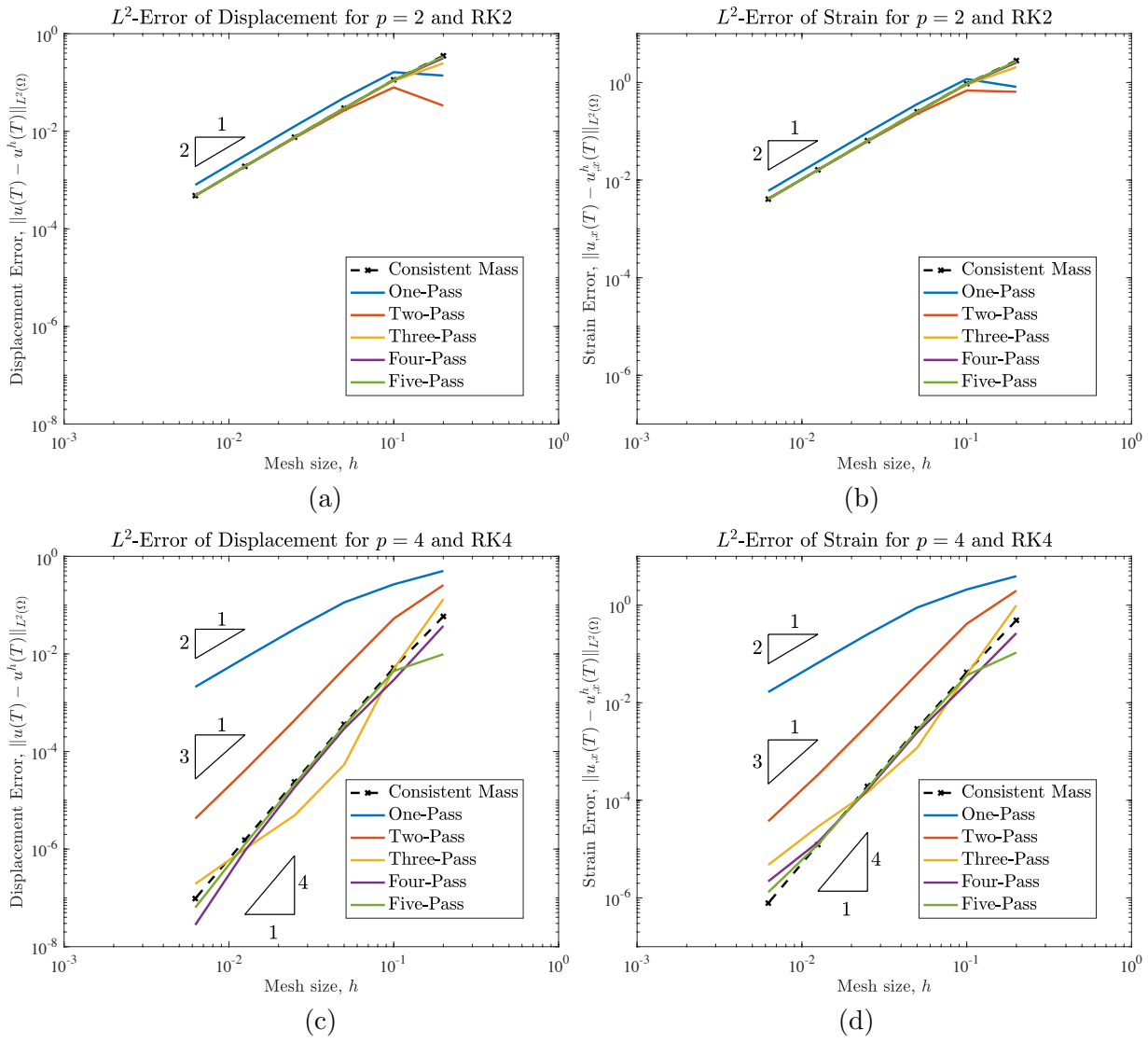

Figure 11: Convergence of explicit isogeometric collocation methods as applied to the clamped-free rod problem. (a) Convergence of displacement for $p = 2$. (b) Convergence of strain for $p = 2$. (c) Convergence of displacement for $p = 4$. (d) Convergence of strain for $p = 4$.

We have solved this problem using a variety of explicit isogeometric collocation methods and a sequence of meshes consisting of 2^2 through 64^2 elements up to a final time of $T = 1.75$. In Fig. 13(a) and (b), we plot the L^2-error in the displacement and strain fields respectively at time $t = T$ as a function of h for $p = 2$ and the second-order Runge-Kutta method. Note that, as with the rod problems, the displacement and strain fields are second-order accurate no matter how many passes are conducted. In Fig. 13(c) and (d), we plot the L^2-error in the displacement and strain fields at time $t = T$ as a function of h for $p = 4$ and the fourth-order Runge-Kutta method. If one corrector pass is carried out, the displacement and strain fields are nearly fourth-order accurate. This is a significant improvement over what was observed for the rod problems. We anticipate that this improvement in accuracy is pre-asymptotic, though we have not seen a slow down in convergence in our numerical experiments. If two corrector passes are carried out, the displacement field is fifth-order accurate, an improvement over what was observed for the rod problems. We anticipate that this improvement in accuracy is pre-asymptotic, though we have not seen a slow down in convergence in our numerical experiments. The strain field is fourth-order accurate if two corrector passes are carried out. If three or more corrector passes are carried out, the displacement field

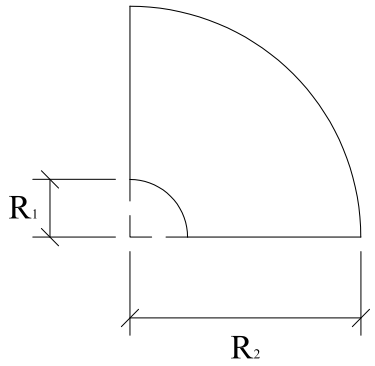

Figure 12: Geometry for the clamped plane-strain quarter annulus problem.

exhibits between fourth- and fifth-order accuracy and the strain field exhibits fourth-order accuracy. In Fig. 13(c) and (d), we plot the L^2-error in the displacement and strain fields at time $t = T$ as a function of h for $p = 6$ and the fifth-order Runge-Kutta method. The results are very similar in behavior to what is observed for $p = 4$ and the fourth-order Runge-Kutta method. Surprisingly, the results for $p = 4$ appear to be better than those for $p = 6$.

7.4. Dynamics of an Elastic Block

For our final example, we consider a 3D elastodynamics problem governing the dynamics of an elastic block occupying the domain $\Omega = (0, 1)^3$. The block is chosen to have density $\rho = 1.0$ and Lamé constants $\mu = 0.5$ and $\lambda = 1.0$. The block is excited by a time-dependent body force, an initial velocity distribution, and prescribed Dirichlet boundary conditions such that the exact solution is as follows:

$$\begin{cases} u_1 = \dfrac{x_1}{4}\sin(\pi x_2)\sin(\pi x_3)\sin(2\pi t) \\ u_2 = \dfrac{1-2x_2}{8}\sin(\pi x_1)\sin(\pi x_3)\sin(2\pi t) \\ u_3 = \dfrac{1-2x_3}{8}\sin(\pi x_1)\sin(\pi x_2)\sin(2\pi t) \end{cases} \tag{7.10}$$

We have solved this problem using $p = 4$, the fourth-order Runge Kutta method, and a sequence of meshes consisting of 2^3 through 64^3 elements up to a time of $T = 0.875$. Unlike the other problems considered in this work, we employed a time-step size of $\Delta t = h/2$ for this problem, which is close in magnitude to the critical time-step size $\Delta t_{\max}$ when five corrector passes are carried out. In Fig. 14(a), we plot the L^2-error in the displacement field at time $t = T$. The displacement field is second-order accurate if one corrector pass is carried out and fourth-order accurate if two or more corrector passes are carried out. The displacement solution improves with an increasing number of corrector passes, though there is little improvement beyond four passes. In Fig. 14(b), we plot the L^2-error in the strain field at time $t = T$. As with the displacement field, the strain field is second-order accurate if one corrector pass is carried out and fourth-order accurate if two or more corrector passes are carried out. In addition, the strain solution improves with an increasing number of corrector passes, though again, there is little improvement beyond four passes. We have also carried out simulations for other polynomial degrees and time-integration schemes and observed similar behavior to what was seen for the clamped-clamped rod problem.

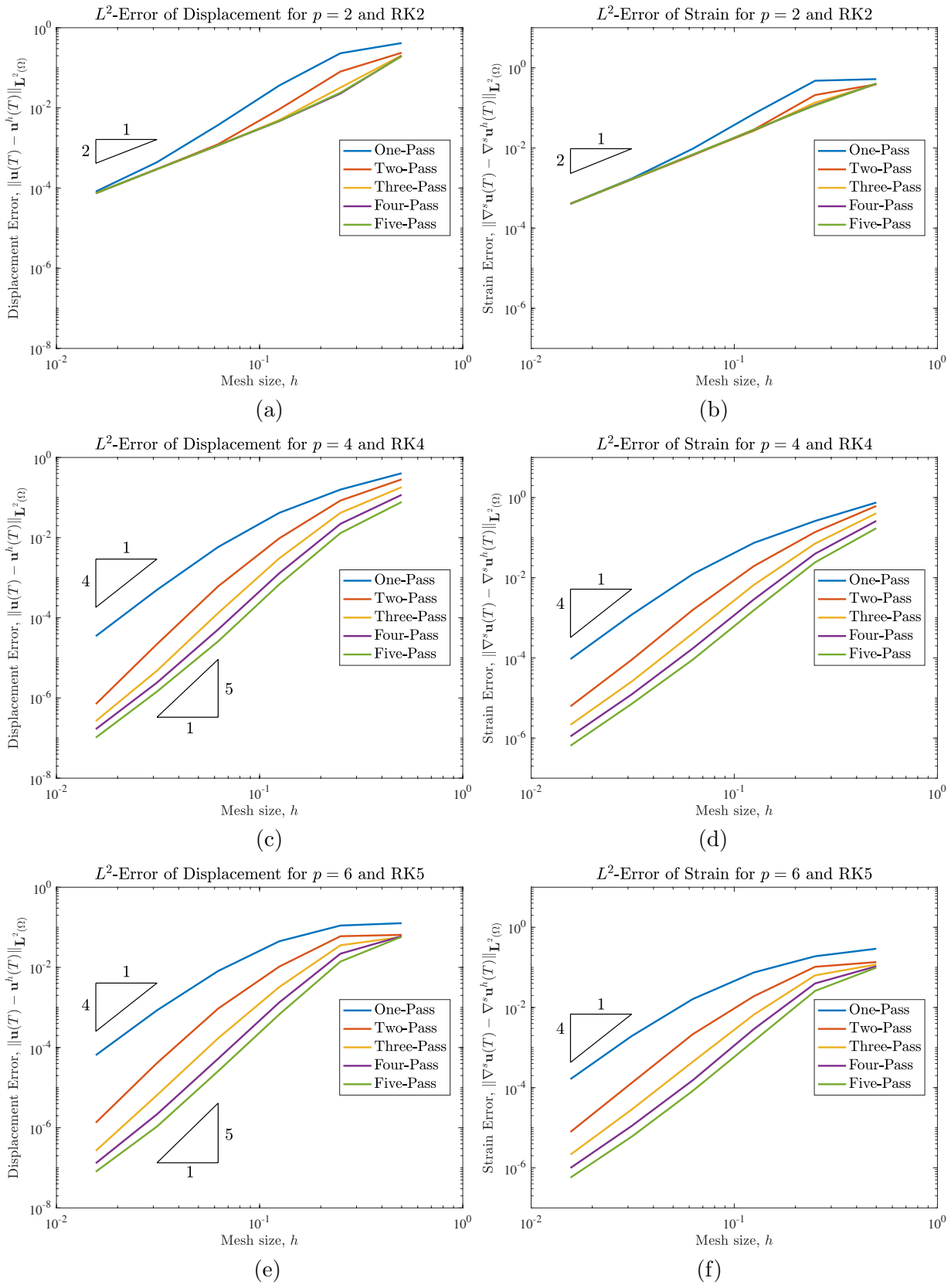

Figure 13: Convergence of explicit isogeometric collocation methods as applied to the clamped plane-strain quarter annulus problem. (a) Convergence of displacement for $p = 2$. (b) Convergence of strain for $p = 2$. (c) Convergence of displacement for $p = 4$. (d) Convergence of strain for $p = 4$. (e) Convergence of displacement for $p = 6$. (f) Convergence of strain for $p = 6$.

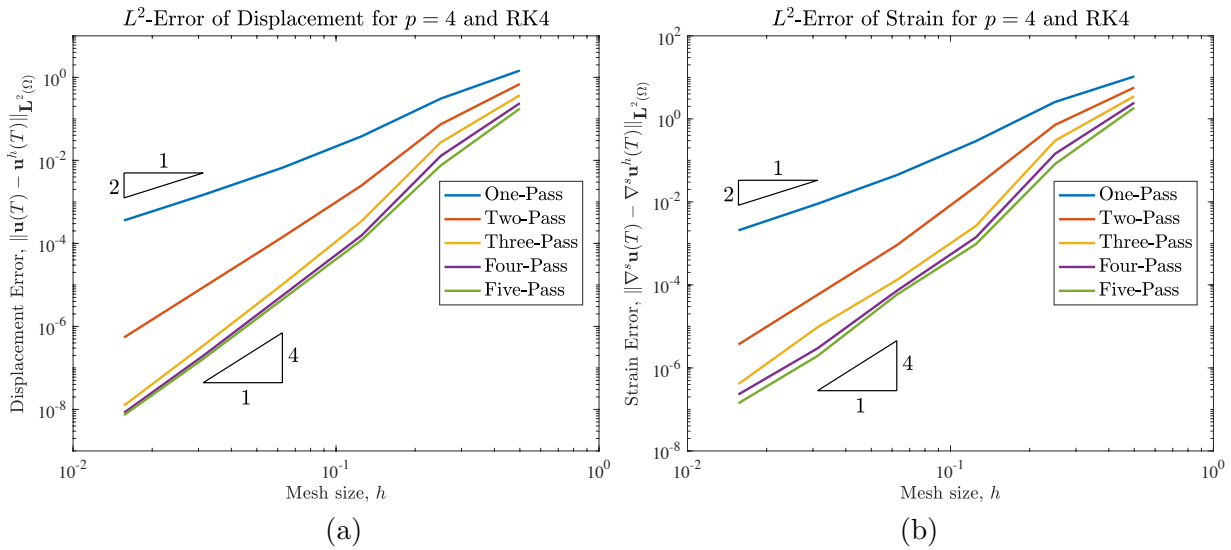

Figure 14: Convergence of explicit isogeometric collocation methods as applied to the elastic block problem. (a) Convergence of displacement for $p = 4$. (b) Convergence of strain for $p = 4$.

8. Conclusions

We have presented a new family of explicit isogeometric collocation methods for structural dynamics which are obtained from predictor-multicorrector schemes. The methods are developed by applying standard explicit time-integration schemes to a semi-discrete isogeometric collocation predictor-multicorrector method. By appealing to spectrum analysis, we characterized the spatial and modal accuracy of the semi-discrete isogeometric collocation predictor-multicorrector method, irrespective of the considered time-integration scheme, as well as the critical time step size for a selection of explicit time-integration schemes. For pure Dirichlet problems, we demonstrated that it is possible to obtain second-, fourth-, and fifth-order accuracy in space with one, two, and three corrector passes, respectively, while for pure Neumann and mixed Dirichlet-Neumann problems, we demonstrated that it is possible to obtain second- and third-order accuracy in space with one and two corrector passes, respectively. Numerical results also revealed that higher-order rates may be obtained pre-asymptotically. We then presented second-order-in-time, fourth-order-in-time, and fifth-order-in-time fully discrete predictor-multicorrector algorithms that are built upon explicit Runge-Kutta methods, and we confirmed the accuracy of these algorithms using a suite of numerical examples in 1D, 2D, and 3D.

Of all the methods presented, the predictor-multicorrector method corresponding to polynomial degree $p = 4$, the classical Runge-Kutta method, and three corrector passes arguably holds the most promise. For pure Dirichlet problems, it provides asymptotic fourth-order accuracy in both the displacement and strain fields, and for pure Neumann and mixed Dirichlet-Neumann problems, it provides fourth-order accuracy in both the displacement and strain fields for practical meshes of interest. Moreover, for the considered suite of numerical examples, the method yields results which are virtually indistinguishable from those obtained using a consistent mass matrix, and the method is robust with respect to both spatial dimension and geometry. In fact, the method yields better results for the clamped plane-strain quarter annulus problem than the predictor-multicorrector method corresponding to polynomial degree $p = 6$, Butcher's fifth-order Runge-Kutta method, and three corrector passes, even though it exhibits a larger critical time-step size and less computational cost per time-step.

While the focus of this paper was on linear elastodynamics, the methods will be extended to the nonlinear setting in future work. It should be mentioned that the methods presented herein harbor great promise for nonlinear structural dynamics where the dominating cost is the evaluation of stress forces. While isogeometric implementations based on Galerkin's method and Gaussian quadrature require $(p+1)^d$

stress evaluations per-degree-of-freedom, isogeometric collocation methods only require one internal force evaluation per-degree-of-freedom [39]. Nonlinear phenomena such as large-deformation contact introduce additional complications, though we expect that the methods presented herein can be combined with recent isogeometric collocation treatments of both frictionless and frictional contact problems [15].

This paper also dealt exclusively with isogeometric collocation methods posed on single-patch geometries, that is, geometries that can be represented through a parameteric mapping defined on the unit square in 2D or the unit cube in 3D. To represent geometries with arbitrary topology, one must turn to the multi-patch concept wherein the geometry is represented through several different parametric mappings [12]. The methods presented herein are easily extended to multi-patch geometries by treating displacement and traction interface conditions between patches in the same manner as Dirichlet and Neumann boundary conditions [4]. Preliminary results demonstrate that second-order and third-order accuracy in space are obtained with one and two corrector passes respectively in the multi-patch setting, and fourth-order-in-space accuracy is obtained pre-asymptotically with three corrector passes. These results are analogous to what was observed herein for pure Neumann and mixed Dirichlet-Neumann problems.

There are a number of potential improvements to our predictor-multicorrector methodology that should be explored in future work. First, improved initial guesses may be employed for the predictor-multicorrector algorithm. Such improvements could be attained through the use of local interpolation techniques [1]. Second, the inverse of the lumped mass matrix may be replaced with high-order approximations of the inverse of the mass matrix [33] within the predictor-multicorrector algorithm. Though this comes with increased cost, preliminary results indicate that optimal convergence rates may be obtained using even a single pass with such an approach. Third, alternative explicit time-discretization schemes such as Runge-Kutta-Nystrom methods [17, 41] may be employed. These schemes are built specifically for second-order systems of ordinary differential equations and exhibit significantly reduced cost in comparison with standard Runge-Kutta procedures. Fourth, the predictor-multicorrector methodology detailed herein may be extended to arrive at implicit-explicit isogeometric collocation methods for structural dynamics [24]. Finally, our algorithms may be applied to isogeometric Galerkin discretizations.

Acknowledgements

J.A. Evans was partially supported by the Air Force Office of Scientific Research under Grant No. FA9550-14-1-0113. A. Reali was partially supported by Fondazione Cariplo - Regione Lombardia through the project "Verso nuovi strumenti di simulazione super veloci ed accurati basati sull'analisi isogeometrica", within the program RST - rafforzamento. T.J.R. Hughes was partially supported by the Office of Naval Research under Grant No. N00014-17-1-2119 and Grant No. N00014-13-1-0500.

References

[1] H. Akima. A new method of interpolation and smooth curve fitting based on local procedures. *Journal of the ACM (JACM)*, 17:589–602, 1970.

[2] P. Antolin, A. Buffa, F. Calabrò, M. Martinelli, and G. Sangalli. Efficient matrix computation for tensor-product isogeometric analysis: The use of sum factorization. *Computer Methods in Applied Mechanics and Engineering*, 285:817–828, 2015.

[3] F. Auricchio, F. Calabro, T.J.R. Hughes, A. Reali, and G. Sangalli. A simple algorithm for obtaining nearly optimal quadrature rules for NURBS-based isogeometric analysis. *Computer Methods in Applied Mechanics and Engineering*, 249:15–27, 2012.

[4] F. Auricchio, L.B. Da Veiga, T.J.R. Hughes, A. Reali, and G. Sangalli. Isogeometric collocation methods. *Mathematical Models and Methods in Applied Sciences*, 20:2075–2107, 2010.

[5] F. Auricchio, L.B. Da Veiga, T.J.R. Hughes, A. Reali, and G. Sangalli. Isogeometric collocation for elastostatics and explicit dynamics. *Computer Methods in Applied Mechanics and Engineering*, 249:2–14, 2012.

[6] S. Balay, S. Abhyankar, M. Adams, J. Brown, P. Brune, K. Buschelman, V. Eijkhout, W. Gropp, D. Kaushik, M. Knepley, et al. PETSc Users Manual Revision 3.5. Technical report, Argonne National Laboratory (ANL), Argonne, IL (United States), 2014.

[7] M. Bartoň and V.M. Calo. Optimal quadrature rules for odd-degree spline spaces and their application to tensor-product-based isogeometric analysis. *Computer Methods in Applied Mechanics and Engineering*, 305:217–240, 2016.

[8] M.J. Borden, M.A. Scott, J.A. Evans, and T.J.R. Hughes. Isogeometric finite element data structures based on Bézier extraction of NURBS. *International Journal for Numerical Methods in Engineering*, 87:15–47, 2011.

[9] J.C. Butcher. On Runge-Kutta processes of high order. *Journal of the Australian Mathematical Society*, 4:179–194, 1964.

[10] F. Calabrò, G. Sangalli, and M. Tani. Fast formation of isogeometric Galerkin matrices by weighted quadrature. *Computer Methods in Applied Mechanics and Engineering*, 316:606–622, 2017.

[11] H. Casquero, L. Liu, Y. Zhang, A. Reali, and H. Gomez. Isogeometric collocation using analysis-suitable T-splines of arbitrary degree. *Computer Methods in Applied Mechanics and Engineering*, 301:164–186, 2016.

[12] J.A. Cottrell, T.J.R. Hughes, and Y. Bazilevs. *Isogeometric Analysis: Toward Integration of CAD and FEA*. John Wiley & Sons, 2009.

[13] J.A. Cottrell, T.J.R. Hughes, and A. Reali. Studies of refinement and continuity in isogeometric structural analysis. *Computer Methods in Applied Mechanics and Engineering*, 196:4160–4183, 2007.

[14] J.A. Cottrell, A. Reali, Y. Bazilevs, and T.J.R. Hughes. Isogeometric analysis of structural vibrations. *Computer Methods in Applied Mechanics and Engineering*, 195:5257–5296, 2006.

[15] L. De Lorenzis, J.A. Evans, T.J.R. Hughes, and A. Reali. Isogeometric collocation: Neumann boundary conditions and contact. *Computer Methods in Applied Mechanics and Engineering*, 284:21–54, 2015.

[16] S. Demko. On the existence of interpolating projections onto spline spaces. *Journal of Approximation Theory*, 43:151–156, 1985.

[17] J.R. Dormand, M.E.A. El-Mikkawy, and P.J. Prince. Families of Runge-Kutta-Nystrom Formulae. *IMA Journal of Numerical Analysis*, 7:235–250, 1987.

[18] H. Gomez and L. De Lorenzis. The variational collocation method. *Computer Methods in Applied Mechanics and Engineering*, 309:152–181, 2016.

[19] M.A. Heroux, R.A. Bartlett, V.E. Howle, R.J. Hoekstra, J.J. Hu, T.G. Kolda, R.B. Lehoucq, K.R. Long, R.P. Pawlowski, E.T. Phipps, et al. An Overview of the Trilinos Project. *ACM Transactions on Mathematical Software (TOMS)*, 31:397–423, 2005.

[20] R.R. Hiemstra, F. Calabrò, D. Schillinger, and T.J.R. Hughes. Optimal and reduced quadrature rules for tensor product and hierarchically refined splines in isogeometric analysis. *Computer Methods in Applied Mechanics and Engineering*, 316:966–1004, 2017.

[21] T.J.R. Hughes. *The Finite Element Method: Linear Static and Dynamic Finite Element Analysis*. Dover, Mineola, New York, 2000.

[22] T.J.R. Hughes, J.A. Evans, and A. Reali. Finite element and NURBS approximations of eigenvalue, boundary-value, and initial-value problems. *Computer Methods in Applied Mechanics and Engineering*, 272:290–320, 2014.

[23] T.J.R. Hughes and W.K. Liu. Implicit-explicit finite elements in transient analysis: Stability theory. *Journal of Applied Mechanics*, 45:371–374, 1978.

[24] T.J.R. Hughes, K.S. Pister, and R.L. Taylor. Implicit-explicit finite elements in nonlinear transient analysis. *Computer Methods in Applied Mechanics and Engineering*, 17:159–182, 1979.

[25] T.J.R. Hughes, A. Reali, and G. Sangalli. Duality and unified analysis of discrete approximations in structural dynamics and wave propagation: Comparison of p-method finite elements with k-method NURBS. *Computer Methods in Applied Mechanics and Engineering*, 197:4104–4124, 2008.

[26] T.J.R. Hughes, A. Reali, and G. Sangalli. Efficient quadrature for NURBS-based isogeometric analysis. *Computer Methods in Applied Mechanics and Engineering*, 199:301–313, 2010.

[27] K.A. Johannessen. Optimal quadrature for univariate and tensor product splines. *Computer Methods in Applied Mechanics and Engineering*, 316:84–99, 2017.

[28] R.W. Johnson. Higher order B-spline collocation at the Greville abscissae. *Applied Numerical Mathematics*, 52:63–75, 2005.

[29] E.J. Kubatko, C. Dawson, and J.J. Westerink. Time step restrictions for Runge–Kutta discontinuous Galerkin methods on triangular grids. *Journal of Computational Physics*, 227:9697–9710, 2008.

[30] W. Kutta. Beitrag zur näherungweisen Integration totaler Differentialgleichungen. 1901.

[31] U. Lee. *Spectral Element method in Structural Dynamics*. John Wiley & Sons, 2009.

[32] S. Lipton, J.A. Evans, Y. Bazilevs, T. Elguedj, and T.J.R. Hughes. Robustness of isogeometric structural discretizations under severe mesh distortion. *Computer Methods in Applied Mechanics and Engineering*, 199:357–373, 2010.

[33] T. Lyche and L.L. Schumaker. Local spline approximation methods. *Journal of Approximation Theory*, 15:294–325, 1975.

[34] C.Barr. Macdonald. *Constructing high-order Runge-Kutta methods with embedded strong-stability-preserving pairs*. PhD thesis, Simon Fraser University, 2003.

[35] C. Manni, A. Reali, and H. Speleers. Isogeometric collocation methods with generalized B-splines. *Computers & Mathematics with Applications*, 70:1659–1675, 2015.

[36] A. Mantzaflaris, B. Jüttler, B.N. Khoromskij, and U. Langer. Low rank tensor methods in Galerkin-based isogeometric analysis. *Computer Methods in Applied Mechanics and Engineering*, 316:1062–1085, 2017.

[37] I. Miranda, R.M. Ferencz, and T.J.R. Hughes. An improved implicit-explicit time integration method for structural dynamics. *Earthquake Engineering & Structural Dynamics*, 18:643–653, 1989.

[38] M. Montardini, G. Sangalli, and L. Tamellini. Optimal-order isogeometric collocation at Galerkin superconvergent points. *Computer Methods in Applied Mechanics and Engineering*, 316:741–757, 2017.

[39] D. Schillinger, J.A. Evans, A. Reali, M.A. Scott, and T.J.R. Hughes. Isogeometric collocation: Cost comparison with Galerkin methods and extension to adaptive hierarchical NURBS discretizations. *Computer Methods in Applied Mechanics and Engineering*, 267:170–232, 2013.

[40] J.W. Thomas. *Numerical Partial Differential Equations: Finite Difference Methods*, volume 22. Springer Science & Business Media, 2013.

[41] P.J. van der Houwen and B.P. Sommeijer. Explicit Runge–Kutta (–Nyström) methods with reduced phase errors for computing oscillating solutions. *SIAM Journal on Numerical Analysis*, 24:595–617, 1987.